# Characterization of evoked compound action potentials in targets of deep brain stimulation for Parkinson's disease

A DISSERTATION
SUBMITTED TO THE FACULTY OF
THE UNIVERSITY OF MINNESOTA BY

Joshua Rosing

IN PARTIAL FULFILLMENT OF THE REQUIREMENTS
FOR THE DEGREE OF
DOCTOR OF PHILOSOPHY

Advisor: Prof. Matthew D. Johnson
October 2022

© Joshua Rosing 2022

# Acknowledgements

I would like to thank every member of my committee for their support and mentorship throughout the development of this dissertation, especially professors Tay Netoff and Matthew Johnson who were instructors for multiple courses of mine – without which I could not have completed this work. The discussions of science with everyone on the committee, whether in class, during meetings, or at conferences, were inspirational and delightful.

I would also like to extend my thanks to my fellow graduate students and siblings in academia in the Johnson lab, especially Alex Doyle, Annie Brinda, Ed Bello, Julia Slopsema, Maripen Yeatts, and Mojgan Goftari. Our conversations were always enjoyable, whether it was science, books, or any other shared interests.

I also give my deepest gratitude to every researcher in the lab who assisted with the non-human primate work: Emily Lecy, Chelsea Spencer, Disa Sullivan, Kelton Wilmerding, Jordan Krieg, Joan Dao, Maddie Blumenfeld, and Sendrea Best – your support made these experiments possible. I also thank Jing Wang, Hannah Baker, and Biswa Mohanty for their assistance in adding another subject to the experiments in Chapter 2.

I thank my parents for their support of my education, and particularly my dad, Mike Rosing, whose decades of mathematics and engineering experience helped me parse through some of the crunchier papers I read.

Finally, I thank my long-time partner and wife, Annie Shao, for always being there for me and supporting me through the busiest and most stressful times of this work and my life.

# Abstract

Deep brain stimulation (DBS) for Parkinson's disease relies on accurate targeting of stimulation to provide the best therapeutic outcomes for patients. Current clinical practices typically rely on a brute force approach to finding the ideal stimulation electrode, and despite improvements to lead geometries such as the inclusion of rows of directional electrodes for precise targeting of stimulation, time constraints often prevent clinicians from making good use of these advancements. Additionally, although research has uncovered specific stimulation targets in common implant areas that are ideal for the treatment of specific symptoms or the avoidance of certain side effects, the clinical capacity for localizing a lead after implantation is not sufficient for confident declarations of implant location, and even the best imaging techniques can only be confirmed with post-mortem histology. Evoked compound action potentials (ECAPs) have been shown to vary by brain region, and to be linked to therapeutic outcomes, but a detailed investigation of their spatiotemporal properties has not yet been conducted.

Through a series of experiments, in parkinsonian non-human primates instrumented with scaled-down clinical DBS leads, ECAP responses to changes in stimulation amplitudes, pulse widths, and electrode configurations were systematically investigated. Additionally, a novel DBS lead with a liquid crystal polymer (LCP) substrate and a high-density array of electrodes with a rough platinum-iridium site coating was evaluated for improved spatial resolution in ECAP and local field potential recordings in DBS targets.

**Project 1:** One challenge with optimizing DBS therapy for a given patient is knowing where electrodes are located relative to the neural pathways around the DBS lead. We tested the hypothesis that ECAP features would differ between electrodes within gray matter (subthalamic nucleus, STN) and white matter (lenticular fasciculus, LF) for STN-DBS implants. ECAPs in these targets were characterized by short-latency 'primary' features (within 1.6 ms of stimulus pulse onset) and longer-latency 'secondary' features (>1.6 ms after stimulus pulse onset). We observed that ECAP primary feature responses were significantly larger in amplitude for LF/LF stimulation/record sites than for STN/STN stimulation/record sites. Furthermore, the number of secondary features detected in the STN (for STN or LF stimulation) was higher than that in LF (for LF stimulation). This supports the concept that ECAP primary features derive from direct axonal activation and secondary features result from post-synaptic axonal activation in

the basal ganglia network. Primary feature amplitude was able to accurately predict electrode location at the border of the lenticular fasciculus and STN within and across all four subjects.

**Project 2:** Another challenge with optimizing DBS therapy for Parkinson's disease has been finding biomarkers that align with the seconds to minutes wash-in effects of DBS therapy on parkinsonian motor signs. ECAP features were found to adapt over the duration of the applied high-frequency DBS pulse train. Primary features habituated over time, while secondary features increased in latency over the first 30 seconds of stimulation, and trended toward earlier latencies at higher stimulation amplitudes. The total increase in secondary feature latency over the 30 seconds following stimulation onset also increased with increasing stimulation amplitude. In comparison to the instantaneous changes in spectral local field potential (LFP) power observed during STN-DBS, the temporal wash-in dynamics of ECAP responses seem to better align with the temporal wash-in profiles of DBS therapy on parkinsonian motor signs, and future studies will need to further investigate correlations between ECAPs and motor signs.

**Project 3:** With the advent of microfabricated technology come opportunities to create bidirectional DBS lead technology to sense and modulate neural activity with higher spatial resolution. To further investigate the spatial features of ECAPs in the basal ganglia, we designed, developed, and evaluated a novel high-density LCP substrate DBS array. The arrays provided improvements in electrode longevity over previous high-density DBS arrays while also providing increased spatial resolution for both ECAP responses and LFP activity compared to state-of-the-art clinical electrodes.

**Table of Contents**

**List of Figures**

# Chapter 1: Introduction

## 1.1 Parkinson's Disease

### 1.1.1 Clinical definition and neuropathology of PD

Parkinson's disease is one of the most commonly occurring movement disorders, affecting roughly 1% of the population over 60 years old [1]. The primary neuropathological cause as it is currently understood is the build-up of misfolded α-synuclein protein caused by environmental factors and highly-heritable gene mutations [2]. This build-up of misfolded proteins occurs throughout the Parkinsonian brain, but the main result is the death of neurons in the brainstem, thalamus, and dopaminergic cells in the substantia nigra, possibly via apoptosis [3], though no single mechanism has yet been confirmed. This loss of cells leads to neural circuit changes throughout the brain that cause motor and cognitive dysfunction and which are treatable through the consumption of dopamine replacement medication, such as levodopa.

### 1.1.2 PD symptoms and clinical rating

The most common symptoms of Parkinson's disease are tremor, rigidity, bradykinesia, and impaired coordination, though cognitive functions including memory, attention, and executive function may also be impaired. Currently, Parkinson's disease is diagnosed via medical history, a neurological and physical examination, and a review of a patient's signs and symptoms [4].

The rating of these signs and symptoms is most commonly performed using the Unified Parkinson's Disease Rating Scale (UPDRS), which is broken into four parts: Intellectual function, mood, and behavior; Activities of daily living; Motor examination; and Motor complications. Each of these parts has subsections that are rated on a scale from 0 to 4, with 0 being a normal, healthy individual and 4 being a severe case. The total of all scores is then calculated to determine the overall severity of the disease [5].

### 1.1.3 Treatment of Parkinson's disease

The majority of cases are able to be treated using levodopa, which can improve most motor symptoms and several cognitive symptoms of the disease. Levodopa is a dopamine precursor that is capable of crossing the blood-brain barrier. Because the symptoms of Parkinson's disease are caused by a loss of dopamine-producing cells in the substantia nigra, the addition of dopamine precursors allows a temporary recovery

from the disease state [6]. However, this treatment is imperfect, and balancing the drug's cycles for the management of motor symptoms can become difficult as the disease progresses, with too little allowing too many untreated symptoms and too much resulting in levodopa-induced dyskinesias [6]. As a result, in later-stage and more severe cases of Parkinson's disease, another therapy is sometimes required.

## 1.2 Clinical outcomes with subthalamic deep brain stimulation

Deep brain stimulation (DBS) is a neurosurgical therapy in which one or more leads of electrodes is implanted into the brain and connected via an extension cable to an implanted neurostimulator. By delivering high-frequency pulsatile stimulation (>100 Hz, typically) to the subthalamic nucleus or globus pallidus, one can reduce parkinsonian motor signs, including bradykinesia, resting tremor, and rigidity [7]. Bradykinesia, or slowness of movement, is another common symptom of Parkinson's disease. It is also associated with difficulty in initiating movements, and a reduction in automatic movements such as eye blinks [8]. DBS is highly effective for treatment of resting tremor, which occurs when the limbs are not in motion or are being held in a pose that does not cause significant postural control against gravity. Resting tremor is most common in the hands, particularly the thumb and forefinger, but can occur in any part of the body and usually starts asymmetrically, with only one side of the body affected. Tremors can range in severity from mild to severe, and can interfere with a wide variety of daily activities, including writing, holding objects, getting dressed, or any other task that requires fine motor ability [9]. DBS can also be effective on muscle rigidity, which is less common in the early stages of Parkinson's disease but can be significant in more advanced stages. The rigidity manifests as stiffness in joints that is beyond what is typical as a result of aging or arthritis [10].

### 1.2.1 Efficacy of subthalamic DBS

DBS therapy for the treatment of Parkinson's disease is typically delivered through the implantation of a DBS lead in the basal ganglia, often in the subthalamic nucleus (STN). The STN was chosen as a target for DBS after early lesioning studies showed that its removal could reverse the symptoms of the disease in non-human primate models [11,12]. More than twenty years later, a review of randomized controlled

trials on the safety and efficacy of DBS for Parkinson's disease found that not only is DBS an effective therapy for treating Parkinson's disease, but it is also superior to other current best medical therapies at controlling motor impairment and disability, quality of life, and reducing medication, though its risk of adverse events was also significantly higher [13]. Another primary benefit of DBS is the consistency of its therapeutic effects. While levodopa treatment can result in fluctuations between over-medication and under-medication states, especially in later-stage Parkinson's disease, DBS provides a more constant therapy given that stimulation is always on.

### 1.2.2 Side effects of DBS

DBS is also not without its own risk of side effects, which can include motor, language, and cognitive effects. While motor side effects such as muscle contractions are easily avoidable in many cases (and are in fact used to set therapeutic stimulation amplitudes), other side effects can be harder to manage. These can include paresthesias (tingling sensations or numbness), dysarthria (speech problems), balance problems, lightheadedness, vision problems, and mood changes including impulsivity and depression [14–16].

## 1.3 Identifying implant location

One of the major challenges in DBS therapy, especially with STN-DBS, is targeting of stimulation to affect neural pathways specific to the disease process while avoiding pathways that can elicit side effects when stimulated. Different brain regions respond differently to stimulation, and placing electrodes properly can be difficult. Implantation in the wrong location or improperly targeting stimulation can lead to lowered side effect thresholds and less effective therapy [17]. Implants for STN-DBS often span the entirety of the STN and include contacts dorsal to the STN, which have been shown to have benefits for reducing dyskinesias while stimulation within the STN on the same leads was shown to exacerbate these dyskinesias [18]. The advent of directional DBS leads has improved our ability to target stimulation, but the increase in numbers of electrodes has brought with it a substantial increase in the amount of time a clinician must spend programming the device – to the point that many clinicians only use directional stimulation as a method of last resort [19–21].

### 1.3.1 Brain imaging

The first method to consider in targeting DBS lead implants is an MRI brain scan [22]. MRI technology has improved greatly in recent years, and the use of 7T imaging allows an accurate definition of the STN [23], which can also be used to create atlases that map to lower resolution 3T MRIs [24]. Pre-operative imaging can allow better placement of the lead during implant than relying on a generic atlas, and post-operative imaging can be done to estimate the final lead location and to assess complications with the implant procedure. However, there is no consensus on which imaging method is the most efficient, and there is no standardized method across implant centers [25]. Additionally, post-operative MRI scanning carries risks with interactions between MRI fields and implanted lead wires as well as a loss of accuracy as the metal in the leads causes artifacts in the imaging that can be difficult to avoid, though some solutions have been proposed [26]. Finally, not all implant centers have access to good imaging technology, and running and maintaining a high-resolution MRI is expensive, preventing this from becoming a standard practice in the near future.

### 1.3.2 Local field potentials in STN-DBS

In STN-DBS research for Parkinson's disease, one popular signal to record and study has been local field potentials (LFPs). LFPs are the summation of local cell membrane potentials, recorded as the electric potential in the extracellular space around neurons. Oscillations in these potentials, particularly in the beta band (roughly 15-35 Hz), have long been linked to Parkinson's disease [27], and have since been proposed as having a key role in motor functions in the cortico-basal ganglia circuit [28]. STN-DBS has been shown to greatly reduce beta oscillations in the STN during stimulation [29], and this suppression has been proposed as a mechanism for DBS therapy in Parkinson's disease as well as a biomarker for closed-loop DBS therapies [30]. However, beta power is also known to decrease during movement, which detracts from its ability to be used as an accurate feedback signal, and suggests the need for another biomarker [31–33].

Beta band LFP power is not the only oscillation in the motor circuits related to motor control. Alpha band activity (roughly 5-15 Hz) has also been shown to play a role in the control of limb movements, and appears to play a different role than that of beta band activity. While beta band power has been shown to decrease with movement

preparation, alpha band power has been shown to increase immediately after a stop signal, leading to the inhibition of movement [34]. These oscillations have also been shown to be heterogeneous throughout the STN, both via high-density electrode recordings [35], and with sensorimotor regions having more beta power and associative regions having more alpha power [36].

### 1.3.3 Microelectrode recordings

Another option for targeting commonly used in implantation is intraoperative microelectrode mapping prior to DBS lead implantation. Although brain atlases and electrode depth can help a clinician target the right area, the precise border of the STN and dorsal axon tracts like the internal capsule, lenticular fasciculus, hyperdirect pathway, and fields of Forel can be determined with intraoperative microelectrode recordings. This can be done using both mean oscillatory activity, and detection of an increase in the noise floor for signals recorded in the STN [37,38]. In fact, the results of high-density microelectrode recordings can be tied to therapeutic outcomes, with a classifier trained on six oscillatory types and interactions capable of predicting likely locations for good therapeutic outcomes [39].

### 1.3.4 Evoked Compound Action Potentials

Another signal recorded in DBS experiments that has also been more recently proposed as a biomarker for closed-loop stimulation therapies is the evoked compound action potential (ECAP): neural responses recorded at the site of or distal to the site of stimulation. ECAPs have been studied and proposed for use in assessing the degree of membrane polarization in peripheral nerves [40], spinal cord [41–43], cochlea [44–47], retina [48,49], and deep brain regions [50,51]. Like LFPs, ECAPs have also been shown to have a connection with DBS therapeutic outcomes, though their link has been less well investigated [51].

Unlike LFPs, ECAPs are thought to arise as a result of axonal activation, and contain much higher frequency information than that observable in LFPs from commercial DBS leads, and have features occurring within milliseconds of stimulus onset and attenuating in amplitude over time [50,52]. ECAPs also have two feature types, primary and secondary. Primary features are very high frequency and higher amplitude than secondary features and have been shown to stem from the immediate, direct axonal activation in response to stimulation. Secondary features, on the other

hand, are thought to result from post-synaptic axonal activation, with the STN-GP network believed to be responsible for their presence during STN-DBS [50,52]. An example of an ECAP response can be seen in Figure 1-1.

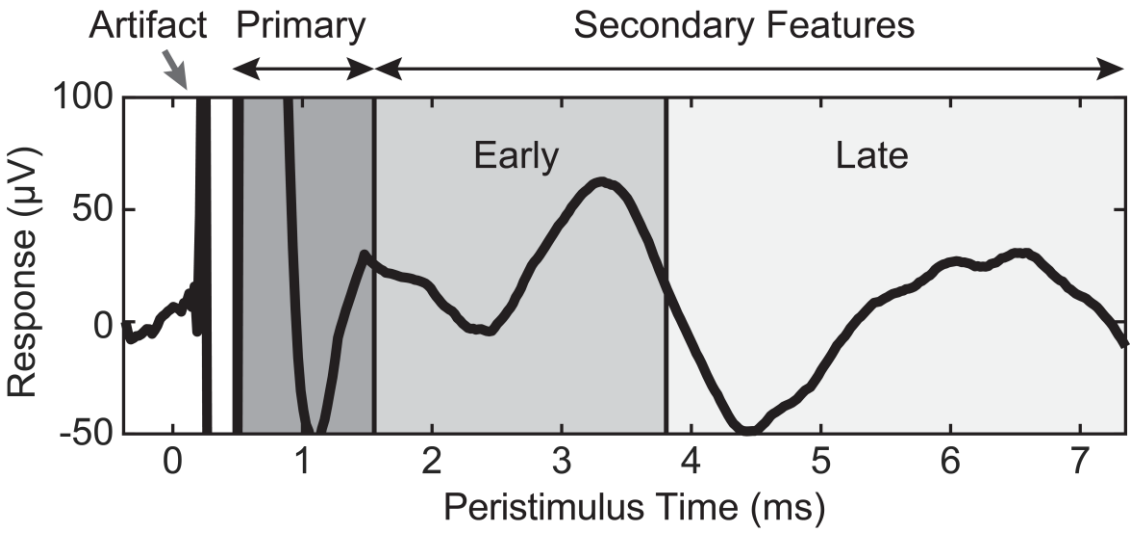


**Figure 1-1** An example ECAP response from STN stimulation. The signal is split into primary and secondary features, with secondary features being further split into early and late features.

The features of ECAP responses and their relationship with underlying neuroanatomical structures makes them a prime subject for investigation to provide an alternative method for implant localization, both during the implant procedure and in providing advanced knowledge for likely therapeutic electrodes to clinicians when performing monopolar reviews and programming patient stimulators.

## 1.4 Statement of Thesis and Chapter Summaries

As a potential biomarker for DBS therapy in Parkinson's disease, it is vital to advance our understanding of the ECAP response to DBS within the basal ganglia. To date, the vast majority of studies on the DBS ECAP response have used bipolar recording configurations from annular DBS leads, leading to poor spatial resolution in the recording of DBS ECAPs. This thesis investigated the spatial and temporal heterogeneity of ECAP responses to stimulation parameters (current amplitude, pulse width, and electrode configuration) using higher density DBS leads including directional

DBS leads with rows of split-band electrodes (Chapters 2 and 3) and a novel high-density DBS array (Chapter 4).

- Chapter 2 describes a study investigating the different qualities of the ECAP response in the STN and surrounding fiber tracts, using the ECAP features to build a linear classifier to predict implant depth.
- Chapter 3 describes a study investigating the temporal aspects of the ECAP response and their differences across stimulation and recording parameters including stimulation amplitude, and stimulation and recording electrode configurations.
- Chapter 4 describes a study evaluating a novel high-density DBS lead technology using a liquid crystal polymer substrate to improve lead longevity during chronic implantation. In this study the spatial heterogeneity of ECAPs in the globus pallidus and putamen were also investigated.

# Chapter 2: Classification of electrically-evoked compound action potentials in the parkinsonian subthalamic nucleus region

Adapted from work submitted to Scientific Reports, “Classification of electrically-evoked compound action potentials in the parkinsonian subthalamic nucleus region”

Joshua Rosing, Alex Doyle, AnneMarie Brinda, Madeline Blumenfeld, Emily Lecy, Chelsea Spencer, Joan Dao, Jordan Krieg, Kelton Wilmerding, Disa Sullivan, Sendréa Best, Biswaranjan Mohanty, Jing Wang, Luke A. Johnson, Jerrold L. Vitek, Matthew D. Johnson

bioRxiv 2022.04.28.489769; doi: https://doi.org/10.1101/2022.04.28.489769

## 2.1 Chapter Overview

Electrically evoked compound action potentials (ECAPs) generated in the subthalamic nucleus (STN) contain features that may be useful for titrating deep brain stimulation (DBS) therapy for Parkinson's disease. Delivering a strong therapeutic effect with DBS therapies, however, relies on selectively targeting neural pathways to avoid inducing side effects. In this study, we investigated the spatiotemporal features of ECAPs in and around the STN across parameter sweeps of stimulation current amplitude, pulse width, and electrode configuration, and used a linear classifier of ECAP responses to predict electrode location. Four non-human primates were implanted unilaterally with either a directional (n=3) or non-directional (n=1) DBS lead targeting the sensorimotor STN. ECAP responses were characterized by primary features (within 1.6 ms after a stimulus pulse) and secondary features (between 1.6-7.4 ms after a stimulus pulse). Using these ECAP features, a linear classifier was able to accurately differentiate electrodes within the STN versus dorsal to the STN in all four subjects. ECAP responses varied systematically with recording and stimulating electrode locations, which provides a subject-specific neuroanatomical basis for selecting electrode configurations in the treatment of Parkinson's disease with DBS therapy.

## 2.2 Introduction

Electrical stimulation within the nervous system is well known to generate evoked compound action potentials (ECAPs) whose features occur within milliseconds of stimulus onset and attenuate in amplitude over time [50,52]. This physiological activity, which is often detected from one or more recording electrodes positioned near the stimulating electrode, reflects the spatial summation of induced membrane polarization adjacent to the recording electrode(s) [53–56]. ECAP features are thought to be indicative of both direct activation of axons (immediate, primary features) as well as synaptic and network-level modulation patterns (delayed, secondary features) [50,52].

Such ECAP features have shown utility for assessing the degree of membrane polarization and thus target engagement with stimulation of the peripheral nerves [40], spinal cord [41–43], cochlea [44–47], retina [48,49], and deep brain regions [50,51]. ECAP features have also been integrated as feedback signals to adjust therapies dynamically, including cochlear implants to streamline behavioral fitting procedures [57]

and spinal cord stimulation to account for changes in the distance between the stimulating electrode(s) and the spinal cord during activities of daily living [42].

Similarly, for DBS applications, knowing the spatial position and orientation of each electrode in the context of the targeted nucleus or fiber pathways can be helpful for fine-tuning stimulation settings [18]. Previous studies have shown that ECAP feature presence and prominence in the subthalamic nucleus (STN) is associated with therapeutic effectiveness in Parkinson's disease [51,58]. However, the degree of spatial heterogeneity of ECAPs within and adjacent to the STN remains unclear. In this study, we investigated the spatiotemporal features of ECAPs in and around the STN in four non-human primates rendered parkinsonian with MPTP treatments and aligned those features to neuroanatomical borders around each DBS lead implant.

# 2.3 Methods

## 2.3.1 Preclinical subjects

This study investigated ECAPs from STN-DBS leads in four aged female rhesus macaque monkeys (*macaca mulatta*; Subjects Ne, Az, So, and Bl; 14.75, 18.5, 19.5, and 26 years old, respectively, at the time of the recordings). Procedures used in the study were approved by the University of Minnesota's Institutional Animal Care and Use Committee and were performed following the United States Public Health Service policy for humane care and use of laboratory animals. All animals received environmental enrichment, free access to water, and a wide variety of foods, including fresh fruits and vegetables. All effort was made to provide animals with adequate care and prevent discomfort during the study.

## 2.3.2 Surgical procedures

Animals were imaged pre-operatively using a 7T or 10.5T human bore magnet with custom-designed head coils for non-human primates at the Center for Magnetic Resonance Research at the University of Minnesota. Similar to previous studies [59,60], DBS leads were implanted along an oblique mapping track that had the largest span of sensorimotor-responsive STN cell activity. The depth of the implant was designed to have electrodes within the sensorimotor STN and the region dorsal to the STN, containing the lenticular fasciculus [61] (**Fig. 2-1**).

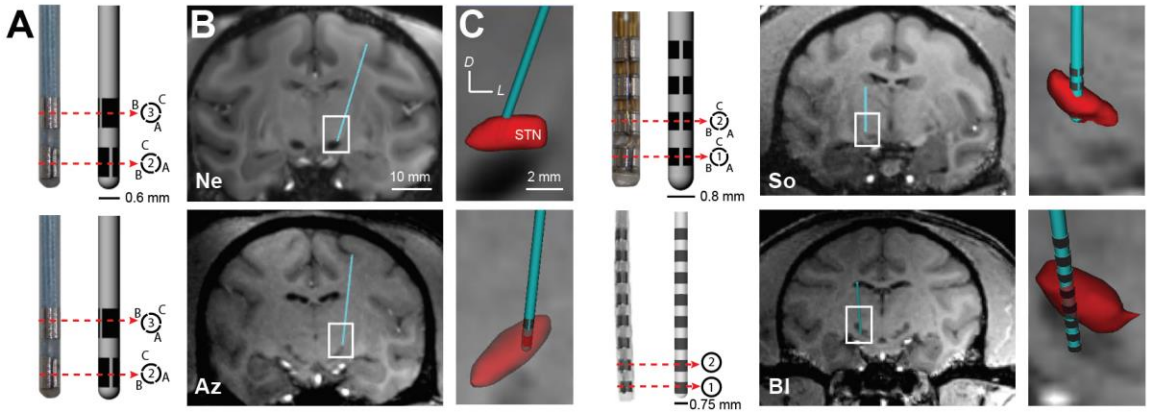


**Figure 2-1** DBS lead localization within the STN. (A) Directional and non-directional DBS leads used in this study. (B, C) High-field 7T or 10.5T MRI and CT co-registration were used to identify the position of each lead within the subthalamic nucleus with confirmation from post-mortem block-face histology.

### 2.3.3 DBS implant procedures

Subjects Ne and Az were implanted with a 6-channel directional DBS lead (Abbott Neuromodulation, 0.6 mm diameter), consisting of 2 rows and 3 columns of electrodes (0.75 mm height, 0.5 mm spacing between rows) with the top row clocked 60 degrees from the bottom row. Subject So was implanted with a 12-channel directional DBS lead (Heraeus Medical Components, 0.8 mm diameter), consisting of 4 rows and 3 columns of electrodes (0.5 mm height, 0.5 mm spacing) with no rotational offset. Subject Bl was implanted with a non-directional DBS lead (NuMed, 0.625 mm diameter) with 8 electrodes (one band electrode per row, 0.5 mm height, and 0.5 mm spacing). DBS lead wires were routed to another chamber to interface with an external neurostimulator (IZ2MH) and recording (PZ5) system (Tucker-Davis Technologies). A CT scan was taken post-implant and co-registered to the pre-operative MRI to estimate placement of the DBS lead implant with respect to the STN (**Fig. 2-1**), and this was confirmed with post-mortem block-face histological imaging. Split-band electrode orientation for Subjects Ne, Az, and So was determined using a post-mortem bubble test whereby the explanted lead, still integrated with the chamber and cap, was submerged in 0.9% saline and stimulated through with 1-5 mA DC current over 1-5 s to generate an electrolysis reaction and small bubble at the stimulated electrode. Range in current and time needed for electrolysis reaction depended on the lead. This was used to verify electrode connector maps, check for electrical shorts, and identify each electrode's orientation

relative to the STN.

### 2.3.4 ECAP stimulation protocol

In each subject, monopolar stimulus pulse trains (125 Hz) were delivered through a single electrode contact using biphasic pulse waveforms that alternated between cathodic or anodic first phase polarities. The first phase had a duration of 100 μs, and the second active recharge phase had a duration of 1 ms with a stimulus amplitude at 10% of the first phase's amplitude. Using these waveforms and pulse trains, the overall stimulus amplitude was increased until sustained side effects were observed on the contralateral side (e.g., muscle contractions, dyskinesias, etc.). Subsequent stimulation trials were then capped at 25 μA below the side effect threshold as determined for each electrode on the DBS lead, with the exception of subject So, in which one experiment was conducted with stimulation amplitudes exceeding dyskinesia side effect thresholds (but remaining below muscle contraction thresholds). During all stimulation trials, the subject was seated and alert while wide-band, monopolar ECAP recordings were collected from the other electrodes at a sampling rate of 48.8 kHz and in reference to cranial bone screws distributed over the parietal lobe.

*Current sweep experiments*: To confirm the existence of ECAPs as neural responses as opposed to electrical artifacts, the current amplitude of the stimulus pulse train was varied randomly between no stimulation and 25 μA below the side effect threshold for each electrode and ECAP feature responses were compared to stimulation artifact for each amplitude. Current sweep data collection trials consisted of 5 seconds of stimulation followed by 5 seconds of no stimulation at each amplitude, with repeated measures of 5 trials per electrode. All current sweep data were collected in a parkinsonian condition.

*Strength-duration sweep experiments*: To further confirm that the signals were of neural origin, strength-duration relationships were assessed through ECAP recordings by systematically varying the current amplitude and pulse width of the charge-balanced, biphasic waveform. The protocol consisted of stimulating at (1) seven current amplitudes (12.5%, 25%, 37.5%, 50%, 62.5%, 75% and 87.5% of side-effect threshold) in the parkinsonian condition, and (2) five pulse widths per stimulus amplitude ranging from 40 to 160 μs for the first phase. Each trial consisted of 30 s of stimulation followed by 30 s without stimulation for each parameter combination. The presentation order of the parameters was randomized but kept consistent across electrodes and subjects (Az and

So).

### 2.3.5 MPTP treatment and evaluation

Each primate was given a series of systemic injections of the neurotoxin MPTP (1-methyl-4-phenyl-1,2,3,6-tetrahydropyridine). Following MPTP treatment, the parkinsonian motor sign severity was rated for each subject using a modified version of the Unified Parkinson's Disease Rating Scale (mUPDRS), which consisted of 14 motor scores, quantified from 0 (no effect) to 3 (severe) [62]. The total motor score for each subject was used to determine the overall severity of parkinsonian motor signs, and these scores were measured at least five times. Averaged scores were 18.25/42 for Subject Ne (moderate), 8.47/42 for Subject Az (mild), 0/42 for Subject So (asymptomatic), and 10.4/27 for Subject Bl (moderate).

### 2.3.6 ECAP processing

Data collected during current sweep and strength-duration sweep experiments were processed to remove the stimulation artifacts and residual noise (**Fig. 2-2**). First, baseline subtraction was applied to each interstimulus ECAP segment (8 ms long) by subtracting the amplitude of the first data point (0.4 ms before the stimulus pulse) from all subsequent data points in the ECAP segment. Next, segments were sorted based on cathodic-anodic or anodic-cathodic stimulus waveforms to ensure that the sample sizes for both stimulus waveforms were identical. For the current sweep experiments, all 5 s of ECAP recordings were averaged together, and for the strength-duration sweep experiments, the last 20 s of the 30 s long ECAP recordings were averaged together [50]. Averaging significantly reduced the electrical artifact as shown in **Fig. 2-2**. The resulting data were then smoothed (4-sample moving average over the first 1.17 ms and 16 sample moving average over the remaining portion of the segment). This two-part filtering approach avoided over-smoothing the primary features while still removing high frequency noise from the secondary features of the ECAP.

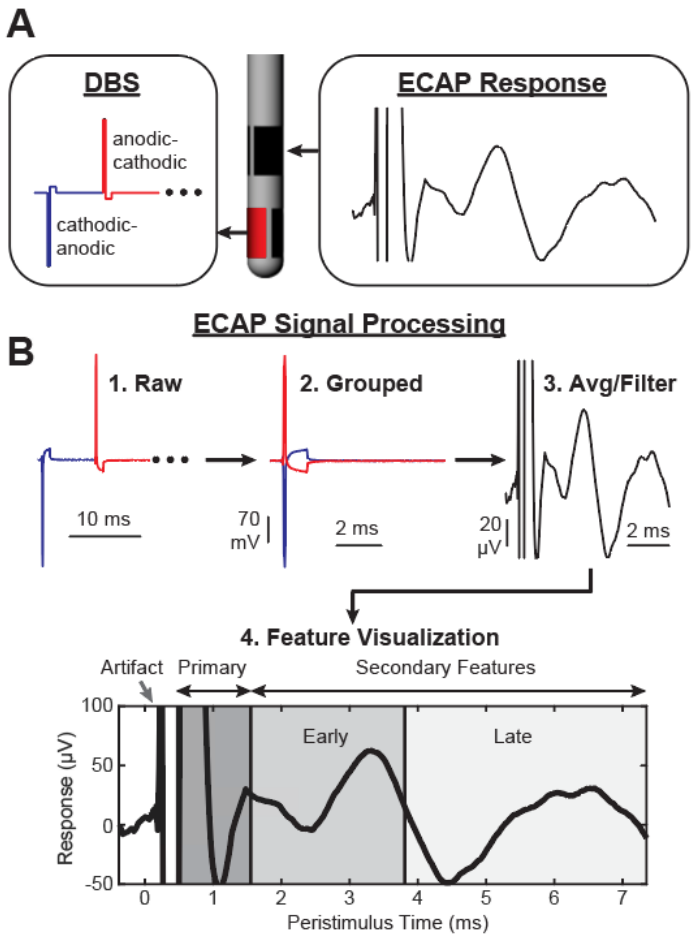


**Figure 2-2** Signal processing of ECAPs within and adjacent to the STN. (A) An alternating sequence of cathodic-leading and anodic-leading waveforms was applied through one electrode while ECAP recordings were collected through all adjacent electrodes. (B) Raw ECAP data were grouped, averaged, filtered, and separated into primary, early secondary, and late secondary features.

Some ECAP recordings, most notably in Subjects Az and So, contained a 0.8-1.0 kHz noise source that was consistent in amplitude over the entire peri-stimulus time window. The peri-stimulus data (from 1.25-7.4 ms) was passed through an IIR filter with 0.99 steepness, with the delayed filter onset designed to avoid generating artifacts in the primary features. The processed data before and after 1.25 ms were then stitched together with a weighted averaging of 9 samples about the stitch to avoid discontinuities in the data (sample 1 was 90% unfiltered sample value plus 10% filtered sample value, and sample 9 was 10% unfiltered sample value plus 90% filtered sample value).

Data with this 0.8-1.0 kHz noise source were marked for filtering objectively as follows. The maximum spectral power in two bands (<500 Hz and 700-1500 Hz) in each recording were calculated and used to define two conditions: (A) the maximum spectral power of the unfiltered <500 Hz band was sufficiently greater (determined by a manually set threshold for each subject) than the maximum spectral power for the unfiltered 700-1500 Hz band, and (B) the maximum spectral power of the unfiltered <500 Hz band was less than the maximum spectral power of the filtered <500 Hz band. If condition A was false, or if both conditions were true, the recording was marked for filtering.

### 2.3.7 Data analysis and classification

ECAP feature windows were determined based on time segments containing similar ECAP responses within and across subjects. Primary features were the first negative and positive peaks to occur, typically within 0.6-1.6 ms of stimulus pulse onset. Secondary features were divided into early (1.6-3.8 ms) and late (3.8-7.4 ms) windows after a stimulus pulse. The separation between early and late windows was based on the transition between stimulus evoked neuronal spike inhibition and a return to a baseline spiking probability with peri-stimulus firing rates of STN neurons during STN-DBS (see [63]). For each ECAP window, the root mean square (RMS) of the data was calculated and then used as feature amplitudes for graphical comparisons, and as features in a linear discriminant analysis classifier. The rationale for feature windows as opposed to defining specific peaks and troughs was based on observations that ECAP features differed in manifestation and in their exact timing across recording configurations for each subject.

A linear classifier (MATLAB) was used to predict stimulation and recording electrode site locations for two possible stimulation/record groups – STN/STN and LF/LF (lenticular fasciculus) – in all subjects. The classifier used all data points from those two groups as samples and training in a leave-one-out approach. Accuracy was calculated from the classification error, was averaged across trials, and compared against chance (50%) to determine effectiveness of the classifier. The classifier was also trained on all data from three subjects and tested using all data from a fourth subject.

Differences in stimulation and recording site location (**Figure 2-6**) were compared individually using MATLAB's *multcompare* function with the Scheffé test for multiple comparisons following a Kruskal-Wallis test (MATLAB's *kruskalwallis* function).

# 2.4 Results

## 2.4.1 Distributions and variability of ECAP features

Within-subject comparison of ECAPs showed high variability of responses across all stimulation parameters (**Fig. 2-3**). Variance was highest during the period of known artifact, and second highest during the earlier portion of the primary feature window. The primary feature window's variance formed a second prominence, suggesting a different source than that of the artifact's variance. Variance declined rapidly during the primary feature window for most subjects, then steadily declined over the early and late secondary feature windows. Most subjects showed much lower variance during the secondary feature windows than during the primary feature window.

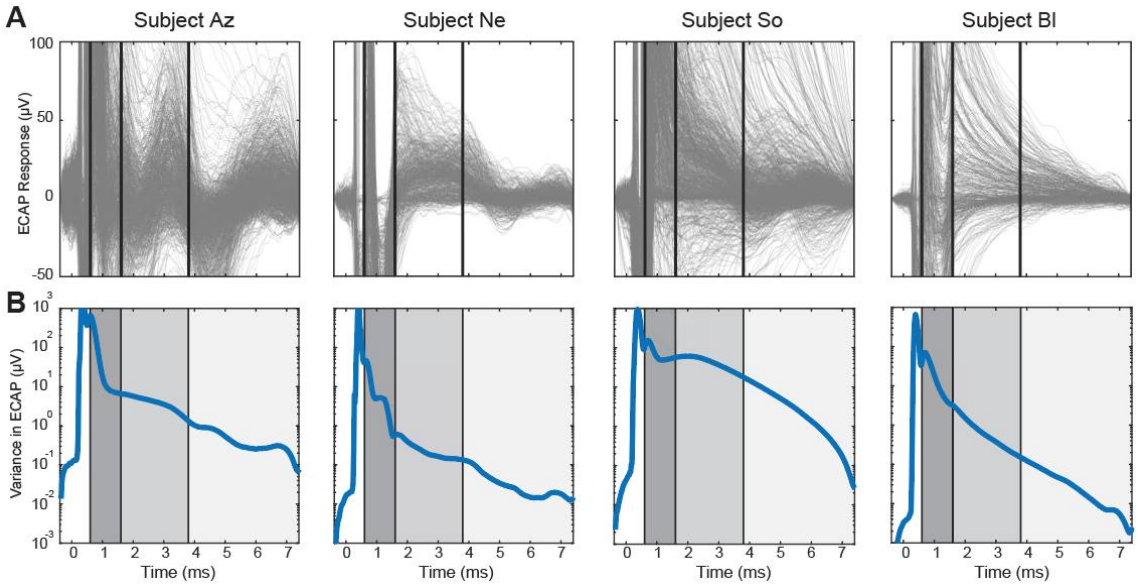


**Figure 2-3** Distributions of all ECAP recordings across subjects. (A) Pooled recordings across tested stimulation pulse widths (subjects Az and So only), amplitudes (all subjects), and electrode configurations (all subjects) for a single recording day. (B) Variance across pooled recordings across the ECAP window. Vertical black lines indicate edges of selected feature windows (primary: 0.6-1.6 ms, early secondary 1.6-3.8 ms, late secondary 3.8-7.4 ms).

### 2.4.2 ECAP responses to varying stimulation amplitudes and pulse widths

Current sweep and pulse width sweep experiments in each of four subjects showed that features of the ECAP response changed non-linearly to adjustments in stimulation parameters while the stimulation artifact increased linearly with increasing stimulation amplitude (**Fig. 2-4**). Features emerged gradually as stimulation amplitude was increased, with secondary features appearing only at stimulation amplitudes that were higher than those sufficient to evoke primary features. Primary and secondary features also generally increased in amplitude with increasing stimulation amplitude (**Fig. 2-4**). ECAP response features also followed classical strength duration curves across stimulation amplitudes and pulse widths (**Fig. 2-5**).

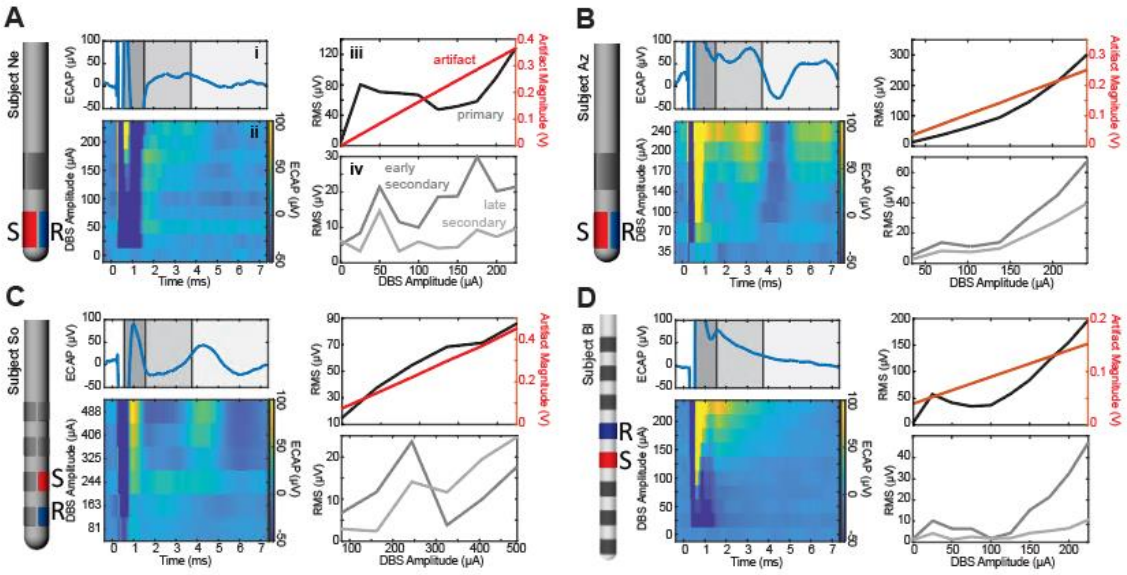


**Figure 2-4** ECAP responses to increasing stimulation amplitudes across all subjects (A-D). (subpanel i) Lead diagrams for each subject with stimulation electrode marked with an S and recording site marked with an R. Example ECAP response to (subpanel ii) the highest stimulation amplitude tested in the MPTP-treated state and (subpanel iii) varying stimulation current amplitudes. RMS values across stimulation amplitudes from epochs containing the (subpanel iv) stimulation artifact and primary features and (subpanel part v) secondary features.

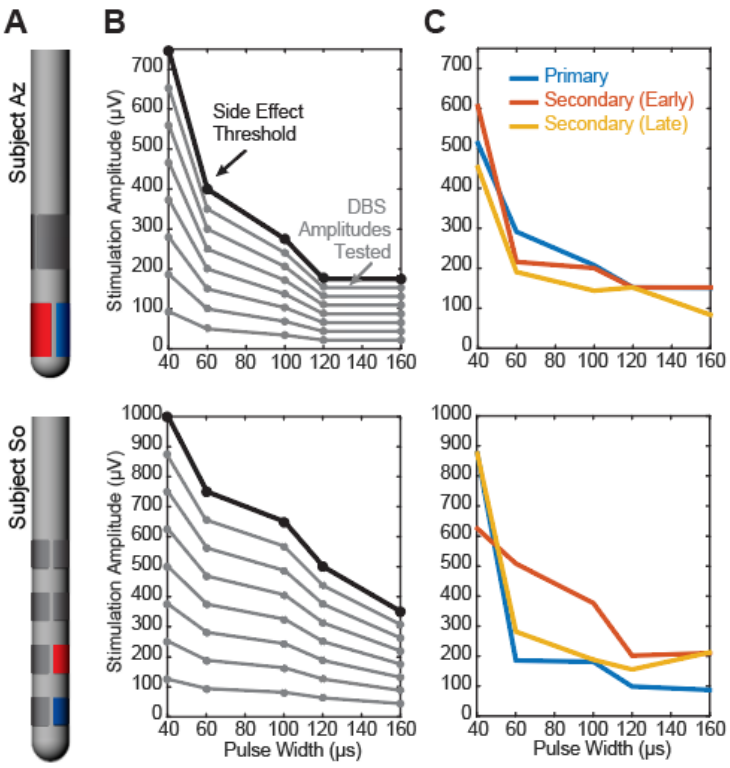


**Figure 2-5** ECAP responses to varying pulse widths. (A) Lead configurations for each subject with the stimulating electrode marked with an S and the recording site marked with an R: 2B/2C for Subject Az and 2B/1B for Subject So. (B) Stimulation amplitudes tested across five pulse widths and eight current levels including the side effect threshold. (C) Stimulation amplitudes and pulse widths necessary to achieve the same primary or secondary feature RMS values within the ECAP response.

### 2.4.3 Spatial Heterogeneity of ECAP Features

Stimulation in the LF produced significantly higher (MATLAB *multcompare* with Scheffe test, p<=0.022) primary feature amplitudes than stimulation in the STN, and LF recording sites during LF stimulation had higher primary feature amplitudes than STN recording sites during LF stimulation (**Fig. 2-6**). Additionally, STN stimulation produced significantly more (MATLAB *multcompare* with Scheffe test, p<0.001) secondary features in subject So than LF stimulation, and STN recording sites also had significantly more detected secondary features than LF sites even during LF stimulation. Mean primary feature amplitudes across subjects were at least 60% lower when recording or stimulating in STN, and an average of 3 secondary features were seen when recording

or stimulating in STN compared to an average of 1.4 when stimulating and recording in LF (**Fig. 2-6**).

The spatial ECAP response differences were readily visible and distinguished by a simple linear classifier (Fig. 2-7). This classifier, trained on all subjects, was capable of correctly determining the stimulation and recording sites as being either both in the STN or both in LF with 95.2% accuracy (measured using the leave-one-out method). Furthermore, when trained on all data from three subjects and tested using data solely from a fourth, the classifier was able to accurately determine the locations of the fourth subject's electrodes with 75% (subject Az), 81.25% (subject So), 100% (subject Bl), and 93.3% (subject Ne) accuracy. This suggests that the DBS ECAP response in both directional and ring electrode configurations can be used to gain an understanding of implant location and is generalizable across subjects. The main determining feature across all subjects was the primary feature amplitude (Fig. 2-7), though there were also visible differences in secondary features in subjects Az and So. Additionally, changes in spatial heterogeneity were observed with changes in stimulation amplitude (Fig. 2-8), with the appearance then disappearance of a dipole as stimulation amplitude increased.

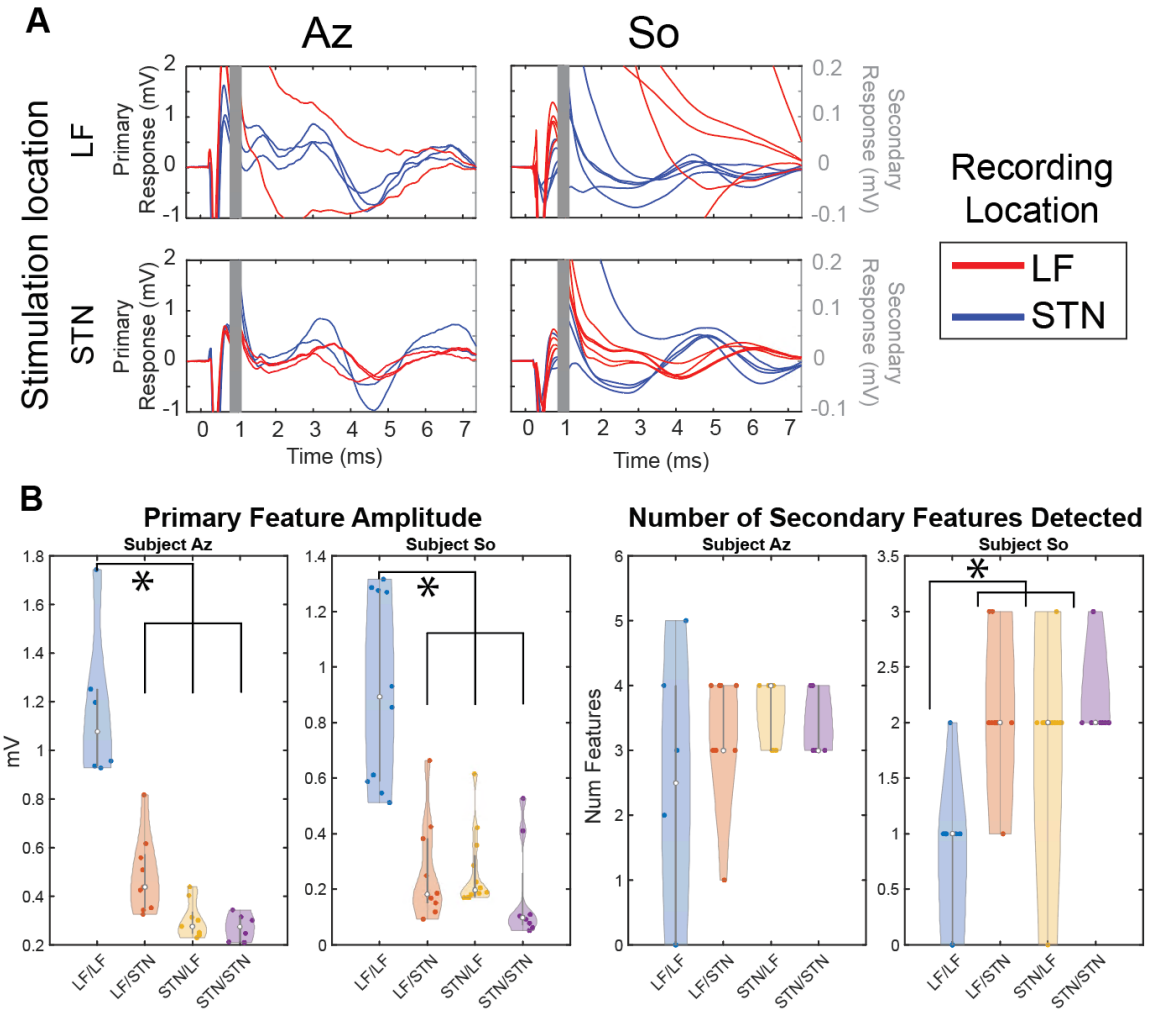


**Figure 2-6** ECAP response by brain region. (A) ECAP responses for all stimulating and recording sites in each subject split by brain region for stimulating (rows) and recording electrodes (colors). In both subjects, STN stimulation with STN recording configuration results in the clearest secondary features, while LF stimulation with LF recording results in the highest amplitude primary features. (B) Quantitative analysis of evoked potentials across all Stimulation/Recording electrode brain regions. Both subjects had significantly lower primary feature amplitudes when recording or stimulating in STN vs the LF/LF group, and subject So had significantly more secondary features detected when stimulating or recording in STN vs the LF/LF group. All significant p values <= 0.022.

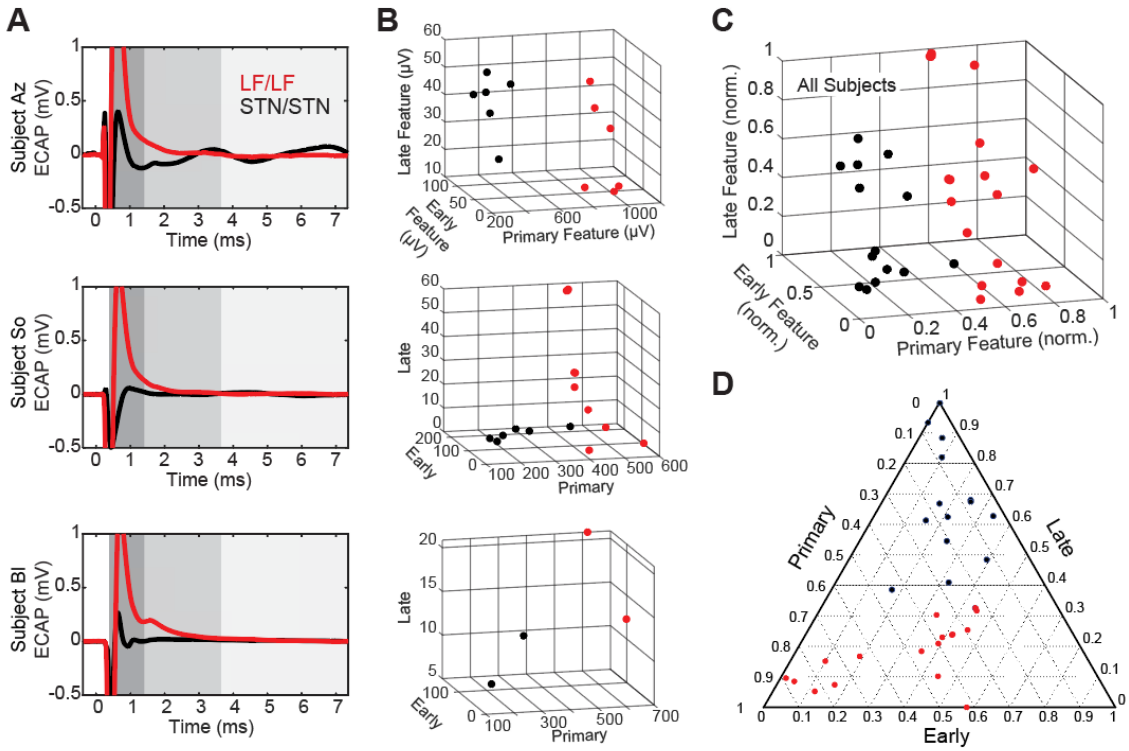


**Figure 2-7** Classification of ECAP responses within and dorsal to the STN. (A) Example ECAP responses for stimulation/recording configurations with STN/STN or LF/LF from subjects Az, So, and Bl. Subject Ne was not included in this figure as all directional DBS electrodes were within the STN. Stimulation amplitudes in each case are similar but not identical within each subject. ECAP responses are shown at a scale for visualizing primary features (dark grey). Early (middle gray) and late (light gray) secondary features were considerably smaller and played a smaller role in differentiating brain regions. (B) Plots of the three RMS features for each subject used by the classifier showing separability of spatial categories (STN/STN, LF/LF) in the feature space. (C,D) RMS values (normalized within subjects) that are plotted together to show separability of spatial categories in feature space.

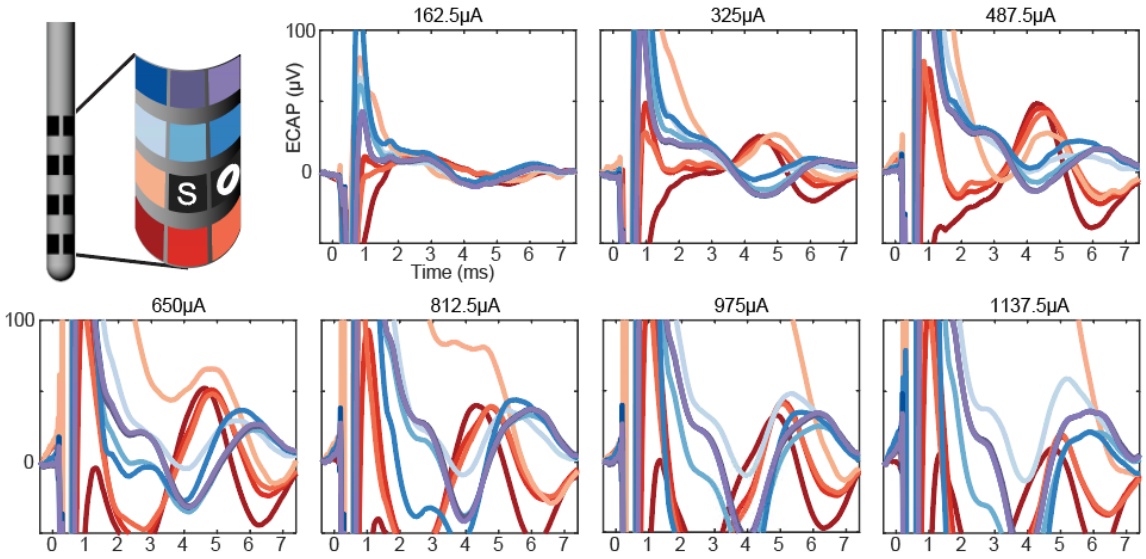


**Figure 2-8** Spatiotemporal changes in ECAP features with increasing stimulation amplitude in Subject So. ECAP responses in each recording channel and a single stimulation site (e2B) to increasing stimulation amplitudes (applied in a randomized order over a single recording session). Side effect threshold for the stimulation site was 650µA. A dipole was present between rows 1/2 and 3/4 from 325µA to 812.5µA. Color grid represents positions of recording sites on lead (unwrapped for 2D representation). O marker indicates an open channel, and S marker indicates the stimulation site.

## 2.5 Discussion

This study investigated the spatiotemporal features of ECAPs collected within and around the STN region in four MPTP-treated non-human primates who were chronically implanted with STN-DBS leads. The use of directional DBS leads in this study enabled multi-channel recordings within and dorsal to the STN in the same subject with electrode contact position and orientation verified with post-mortem histology. ECAP features in the STN region were observed to (a) follow a nonlinear intensity curve with respect to stimulation amplitude; (b) exhibit strength-duration curve relationships; and (c) vary systematically by stimulation / recording electrode configurations. Findings (a) and (b) provide continued support for the neurobiological basis of ECAPs in the STN region, while finding (c) indicates an opportunity to use subject-agnostic analysis methods of ECAP responses to determine electrode positions using pooled multi-subject classifiers.

Traditionally, ECAP features have been viewed as having specific peak and

trough features [50–52,54,64] that reflect detection of neural sources of convergent activity. In this study, the timing, location, and number of these features varied depending on stimulation amplitude and electrode configuration, lead geometry, and implant location. Using time ranges rather than specific points when calculating ECAP features allowed for more broadly applicable data analyses such as the use of summary statistics (RMS values), rather than peak-to-trough amplitudes or prominences. Additionally, previous ECAP studies have relied on macroscale electrodes and bipolar recording configurations with two electrodes guarding a center stimulating electrode [50,51,64]. In this study, single-electrode ECAP responses were used to show visually separable features between the STN and regions dorsal to the STN, most prominently observed in the primary features. These features enabled classifying electrode location (within the subthalamic nucleus or within the lenticular fasciculus) with high accuracy across subjects.

Previous research has suggested that the likely source of the primary features are direct axonal activation of passing white matter fibers [52], which would be in much greater number and more aligned in the LF than in the STN. This may provide one possible explanation for why the primary feature amplitude was larger in the LF/LF than the STN/STN configurations. Though the ECAP response data did not support a method to determine DBS lead orientation, such as the use of a directional classifier, additional subjects and recordings spanning a broader set of implant locations would be helpful to tease apart the neuroanatomical origins of differences in directional ECAP responses (**Fig. 2-7**, **Fig. 2-8**). Additionally, the classifier was not used to predict whether a stimulating electrode was in the STN while the recording electrode was in the LF or vice versa given that stimulating and recording electrode pairs in the same region proved to have a much higher accuracy level.

The ability of a linear classifier to accurately predict where a stimulation and recording site pair are located could be useful for programming DBS systems, especially as DBS lead designs become more complex and clinical monopolar reviews take longer to complete. Studies have shown that stimulation targeting specific regions about the STN can be helpful in the programming process. For example, the dorsal region above STN can be beneficial for the cardinal motor signs of PD including rigidity and bradykinesia [65], but also helpful for suppressing stimulation-induced dyskinesias [18]. At the same time, stimulation of the lenticular fasciculus has been associated with worsening of gait parameters [66] and worsening of freezing of gait [67].

This approach complements other techniques for identifying DBS lead position and offers some strong advantages. One common approach is to merge high-field pre-operative MR imaging, that can visualize boundaries of the STN [68], with post-operative CT imaging showing the position of the lead within the context of the cranium and ventricles. Most DBS centers, however, do not have access to high-field MRI, and even with such imaging facilities the definitive location and orientation of the DBS lead implant can only be confirmed, as shown in this study, with post-mortem histology. Previous studies have also shown that resting-state local field potentials filtered in the beta-band (12-30 Hz) can be useful for intra-operative targeting of DBS lead implants in the dorsolateral 'motor' STN, but again the exact location of the spectral feature can vary by several millimeters, especially considering the necessity to use bipolar electrode montages [69]. In this way, the ECAP approach may be a valuable complement for clinicians to use with current methods.

The use of alternating polarity stimulation as a means of canceling stimulation artifact meant the stimulation parameters differed slightly from what is used clinically. In some studies, using artifact removal hardware for thalamic ECAP recordings suggested that the anodic-leading and cathodic-leading ECAP responses and therapeutic effect on tremor were largely similar [64]. Other studies using cochlear stimulation [70] have indicated differences in ECAP responses between anodic-leading and cathodic-leading pulses. As such, the ECAP signals recorded may reflect an amalgam of different sources evoked between waveform polarities. However, any such amalgamation does not impact the usefulness of the ECAP features for electrode localization using a linear classifier. Some, but not all, recordings also contained high-frequency noise in the 0.8-1.0 kHz range, which necessitated offline filtering. While the approach removed most of the high-frequency noise, some recordings still had a small residual noise level remaining. By employing analysis techniques such as calculation of RMS values as our feature amplitude metric, we reduced the effect that any residual noise had on the analysis, since the noise was of a high enough frequency to have multiple periods within a given feature window and features were either positive enough or negative enough that the noise did not cause the signal to cross 0 (thus the RMS of the noise approached a net 0 change on the signal).

## 2.6 Conclusion

This study found several principles that govern ECAP responses to DBS targeted within and around the STN. Increased stimulation amplitude or pulse width primarily affected the amplitude of ECAP features so long as the stimulation parameter exceeded a threshold to produce a detectable response feature. In contrast, variation in stimulation and recording site configurations had a large effect on when and what features were present in the ECAP response. Importantly, primary feature amplitude provided a means to accurately distinguish electrode contacts within or dorsal to the STN, which will be useful for guiding the programming of STN-DBS systems in the future.

# Chapter 3: Investigation of evoked compound action potential dynamics in the parkinsonian subthalamic nucleus region

## 3.1 Chapter Overview

Prior investigation of evoked compound action potentials (ECAPs) during deep brain stimulation (DBS) has primarily focused on the existence of ECAPs as biological signals and how ECAP features change with increasing stimulation amplitude. Future closed-loop systems that utilize features of ECAPs would benefit from a more detailed understanding of the extent to which ECAP features adapt after the onset of stimulation. In this study, we investigated the short-term time-course of changes in ECAP features in the subthalamic nucleus and lenticular fasciculus of two MPTP-treated non-human primates. Over the initial thirty seconds of stimulation, the primary features of the ECAP response within both regions habituated over time (median range: 8-14%), whereas the secondary features showed a longer latency (~0.5 ms, time constant median range: 5-12 sec) after each stimulus pulse. These results suggest an initial decrease in the fidelity of axonal entrainment to the stimulus pulse train (primary features) as well as some combination of axonal conduction and synaptic delay in the basal ganglia network. Such time constants are on the same order of magnitude as many of the reported wash-in effects of STN-DBS therapy on parkinsonian motor signs.

## 3.2 Introduction

Deep brain stimulation (DBS) targeting the subthalamic nucleus (STN) for treating the motor signs of Parkinson's disease is known to result in neural circuit changes that adapt over time following stimulation onset [71]. Previous studies have focused on investigating these changes in neuronal spike rates and patterns within the globus pallidus, which receives excitatory projections from STN and sends inhibitory projections to the STN. These studies have shown that STN-DBS generates an increase in globus pallidus spike activity with the effect waning over time [72], and that STN-DBS generates phase-locked spike activity in the globus pallidus, the fidelity of which also wanes over time [73]. In contrast, STN-DBS reduces neuronal spike activity in the STN [63,74], and beta band power reduction in recorded local field potentials (LFPs) has been suggested as a potential physiological feature of deep brain stimulation (DBS) therapy [75,76]. The reduction observed in the STN is almost instantaneous with the onset of stimulation [77] and nearly instantaneously in the globus pallidus [78].

These time ranges for electrophysiological effects of STN-DBS to wash-in mirror similar time ranges for the therapeutic effects of STN-DBS on parkinsonian motor signs to manifest. For instance, STN-DBS effects on resting tremor typically occur within a few seconds [79], whereas effects on muscle rigidity and bradykinesia can require seconds to minutes to take hold [80]. Additionally, STN-DBS can improve bradykinesia with effects that are both concurrent with stimulation as well as effects that have a wash-in time constant on the order of minutes [81].

Features of electrically-evoked compound action potentials (ECAPs) that correspond to both local activation (primary features occurring within 1-2 ms of a stimulus pulse) and network modulation (secondary features occurring after the primary features) have been investigated in terms of their biological existence and relationship to therapy on parkinsonian motor signs [51,52,54,64]. While some work has been done investigating the temporal dynamics of ECAPs in the globus pallidus during STN-DBS [50], this work was limited to single stimulation sites, amplitudes, and recording configurations. Additionally, the extent to which ECAP features in the STN during STN-DBS adapt after stimulation onset is not known.

In this study, we investigated the temporal changes in ECAP features in the STN and lenticular fasciculus (LF) of two MPTP-treated non-human primates over the course of thirty seconds of stimulation. We further investigated how these temporal changes depended on stimulus amplitudes, pulse widths, and electrode configurations. Such knowledge will be critical to future closed-loop DBS systems that utilize ECAP features as feedback for titrating stimulation settings.

## 3.3 Methods

### 3.3.1 Preclinical subjects

ECAPs from two aged female rhesus macaque monkeys (*macaca mulatta*; subjects Az, aged 18.5 years, and So, aged 19.5 years) were investigated in this study using STN-DBS leads. Procedures used in the study were approved by the University of Minnesota's Institutional Animal Care and Use Committee and were performed following the United States Public Health Service policy for humane care and use of laboratory animals. All animals received environmental enrichment, free access to water, and a wide variety of foods, including fresh fruits and vegetables. All effort was made to provide animals with adequate care and prevent discomfort during the study.

### 3.3.2 Surgical Procedures

Pre-operative imaging using a 7T human bore magnet with custom-designed head coils for non-human primates at the Center for Magnetic Resonance Research at the University of Minnesota was performed for each subject. DBS leads were implanted along an oblique mapping track that had the largest span of sensorimotor-responsive STN cell activity, matching previous studies [21,22]. Implant depths were designed to have electrodes within the sensorimotor STN and the region dorsal to the STN, containing the lenticular fasciculus [23] (**Fig. 3-1**).

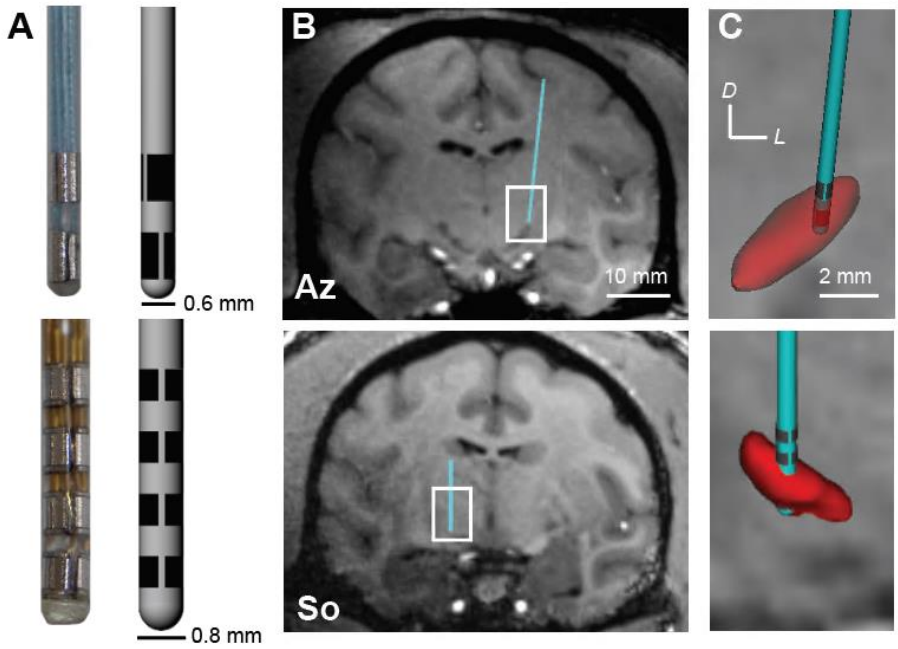


**Figure 3-1** DBS lead localization within the STN. (A) Directional DBS leads used in this study. (B, C) High-field 7T MRI and CT co-registration were used to identify the position of each lead within the subthalamic nucleus with confirmation from post-mortem block-face histology.

### 3.3.3 DBS Implant Procedures

A 6-channel directional DBS lead (Abbott Neuromodulation, 0.6 mm diameter), consisting of 2 rows and 3 columns of electrodes (0.75 mm height, 0.5mm spacing between rows) with the top row clocked 60 degrees from the bottom row was implanted in subject Az. A 12-channel directional DBS lead (Heraeus Medical Components, 0.8

mm diameter), consisting of 4 rows and 3 columns of electrodes (0.5 mm height, 0.5 mm spacing) with no rotational offset was implanted in subject So. DBS lead wires were routed to another chamber to interface with an external neurostimulator (IZ2MH) and recording (PZ5) system (Tucker-Davis Technologies). To estimate placement of the DBS lead implant with respect to the STN, a post-operative CT scan was taken and co-registered to the pre-operative MRI (**Fig. 3-1**). Lead location was later confirmed with post-mortem block-face histological imaging. A post-mortem bubble test was used to determine split-band electrode orientation, verify electrode connector maps, check for electrical shorts, and identify each electrode's orientation relative to the brain. In this test, the explanted lead (still integrated with the chamber and cap) was submerged in 0.9% saline, and stimulated through with 1-5 mA DC current over 1-5 sec to generate an electrolysis reaction and small bubble at the stimulated electrode, with different currents and durations required for each lead.

### 3.3.4 ECAP Stimulation Protocol

Pulse trains (125 Hz) of monopolar stimulation were delivered through a single electrode contact. These pulse trains consisted of biphasic pulse waveforms that alternated between cathodic and anodic for first phase polarities. The first phase of each pulse had a duration of 100 µs, while the second (active recharge) phase had a duration of 1 ms with a stimulation amplitude at 10% of the first phase's amplitude. The overall stimulation amplitude was increased until sustained side effects were observed on the contralateral side (e.g., muscle contractions, dyskinesias, etc.). Subsequent stimulation trials were then capped at 25 µA below the side effect threshold as determined for each electrode on the DBS lead, except in the case of subject So where ECAPs were recorded transiently at higher amplitude settings during dyskinesias. Monopolar ECAP recordings were collected from non-stimulating electrodes at a sampling rate of 48.8 kHz and in reference to cranial bone screws distributed over the parietal lobe during each stimulation trial.

*Strength-duration sweep experiments*: Systematic variation of current amplitude and pulse width of the charge-balanced, biphasic waveforms was used to assess strength-duration relationships. The protocol consisted of stimulating at (1) seven current amplitudes in the parkinsonian condition, and (2) five pulse widths per stimulus amplitude ranging from 40 to 160 µs for the first phase. Each trial consisted of 30 s of stimulation, with 30 s of no stimulation between each parameter combination. The order

in which the parameters were delivered was randomized, but kept consistent across electrodes and subjects (Az and So). Stimulation amplitudes were kept below side effect threshold (12.5%, 25%, 37.5%, 50%, 62.5%, 75% and 87.5% of side-effect threshold), except in the case of subject So, in which side effects thresholds for dyskinesias were exceeded for an additional experiment with higher amplitude stimulation (25%, 50%, 75%, 100%, 125%, 150%, and 175% of side effect threshold). These stimulation amplitudes were still below muscle contraction side effect thresholds.

### 3.3.5 MPTP treatment and evaluation

A series of systemic injections of the neurotoxin MPTP (1-methyl-4-phenyl-1,2,3,6-tetrahydropyridine) was given to each animal. Following MPTP treatment, the parkinsonian motor sign severity was rated for each subject using a modified version of the Unified Parkinson's Disease Rating Scale (mUPDRS). mUPDRS consisted of 14 motor scores quantified from 0 (no effect) to 3 (severe) [24]. Overall severity of parkinsonian motor signs was determined using the total motor score for each subject, and these scores were measured at least five times. Averaged scores were 8.47/42 for subject Az (mild), and 0/42 for subject So (asymptomatic).

### 3.3.6 ECAP processing

Data were processed to remove the stimulation artifacts and residual noise using a two-part filtering approach to avoid over-smoothing primary features while removing high frequency noise from secondary features of the ECAP (**Fig. 3-2**). First, baseline subtraction was applied to each interstimulus ECAP segment (8 ms long) by subtracting the amplitude of the first data point (0.4 ms before the stimulus pulse) from all subsequent data points in the ECAP segment. ECAPs were then calculated over the course of stimulation using a 100-pulse (0.8 second) window to average recorded potentials and reduce noise. This window was slid by 10 pulses at each time point (0.08 seconds). This averaging dramatically reduced the electrical artifact as shown in **Fig. 3-2**. Finally, the resulting data in each window were smoothed (4-sample moving average over the first 1.17 ms and 16 sample moving average over the remaining portion of the segment).

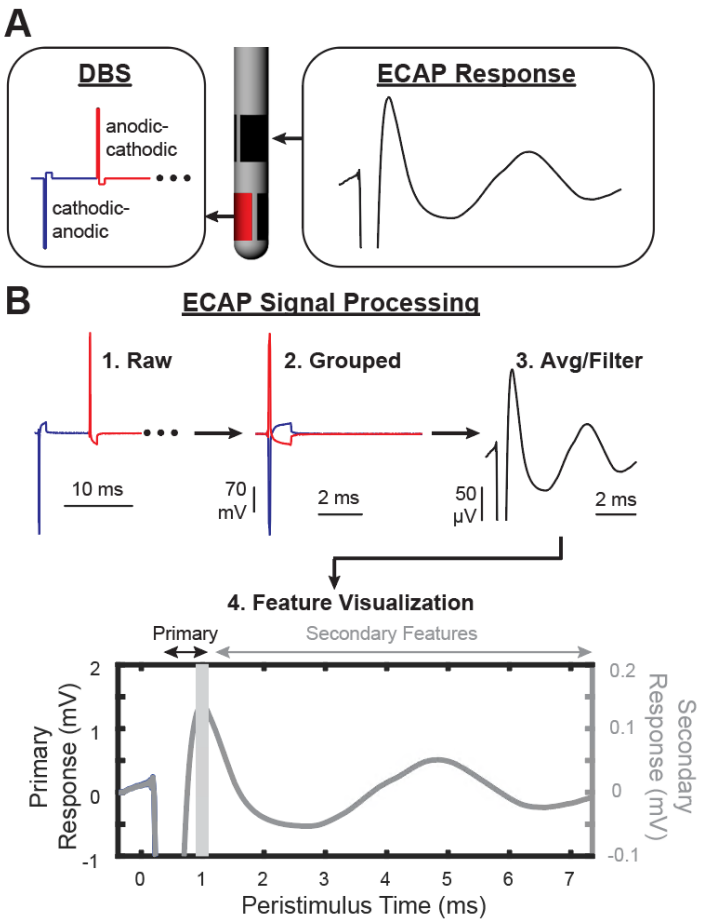


**Figure 3-2** Signal processing of ECAPs within and adjacent to the STN. (A) ECAP recordings were collected through non-stimulating electrodes during an alternating sequence of cathodic-leading and anodic-leading waveforms applied through one electrode. (B) Raw ECAP data were then grouped by leading stimulation polarity, averaged, filtered, and separated into primary and secondary features.

A 0.8-1.0 kHz noise source that was consistent in amplitude over the entire peri-stimulus time window was detected in some ECAP recordings. To avoid generating artifacts in the primary features during filtering, the peri-stimulus data was passed through an IIR filter with 0.99 steepness with a delayed filter onset (only data from 1.25-7.4 ms was filtered). A weighted averaging of 9 samples was used to stitch the processed data before and after 1.25 ms together to avoid discontinuities in the data (sample 1 was 90% unfiltered sample value plus 10% filtered sample value, and sample 9 was 10% unfiltered sample value plus 90% filtered sample value).

The need for filtering of data with this 0.8-1.0 kHz noise source was determined objectively as follows. Two conditions were defined using the calculated maximum spectral power in two bands (<500 Hz and 700-1500 Hz) in each recording: (A) the maximum spectral power of the unfiltered <500 Hz band was sufficiently greater (determined by a manually set threshold for each subject) than the maximum spectral power for the unfiltered 700-1500 Hz band, and (B) the maximum spectral power of the unfiltered <500 Hz band was less than the maximum spectral power of the filtered <500 Hz band. If condition A was false, or if both conditions were true, the recording was marked for filtering. This detection was run using data averaged over the last 20 seconds of stimulation, then applied to all windows of data in that recording to make the process computationally efficient.

### 3.3.7 Data analysis

*Feature detection:* Primary feature amplitudes were determined as the maximum and minimum values within the time range of 0.33 ms to 1.13 ms post-stimulus onset, while secondary feature latencies were detected using a guided *findpeaks* approach over 1.25 ms to 7.40 ms post-stimulus onset to exclude false positives, including the use of a minimum peak prominence based on signal maximum in the secondary feature time window and a minimum peak distance of 1.1 ms. Negative secondary features were detected using the negative of the response. Detected features were further filtered based on the time at which they occurred and via cluster analysis (MATLAB *clusterdata*) to ensure proper tracking of the same feature across the entire stimulation duration.

*Curve fitting:* After feature detection, features were modeled using a sigmoid curve fit with 5 parameters. A noise signal of approximately 0.4 Hz was detected throughout most recordings in the stimulation duration axis. This was filtered prior to fitting a curve using a lowpass IIR filter with 0.9 steepness. Using this filter required continuous data, so any time points where a feature was not detected (this was never the case for primary features) were linearly interpolated. The filtered data was then used for all future analysis.

Starting points and parameter bounds for the model were set based on the typical requirements for a good fit across all data. This resulted in a model that fit a curve for a decaying sigmoid to the data. Sigmoid fit was further encouraged through including baseline data points prior to the onset of stimulation, calculated as the mean of the first 15 data points (first 1.2 seconds of stimulation) to represent an initial steady state.

Goodness of fit was measured using the $R^2$ value calculated using only the measured data (excluding the "pre-stimulation" additions) to ensure the addition of estimated data did not bias the fit. The starting and ending points of the data were also weighted higher than the middle points for the secondary features, applying a weight of 1 for samples in the first 4.8 seconds, a weight of 1.5 for samples in the last 1.6 seconds, and a weight of 0.5 for all remaining samples.

Two types of sigmoid models were applied: Model 1 was defined as the type that best fit the majority of a given feature, while Model 2 was defined as its polar opposite. For primary feature amplitudes, Model 1 was a decaying sigmoid ( $\frac{a}{b+e^{c*x-d}} + e$) where c was bound as a negative value with Model 2 being a growing sigmoid (c bound as a positive value). Secondary feature latency Model 1 was a growing sigmoid while secondary feature latency Model 2 was a decaying sigmoid.

*Feature analysis:* Using the sigmoidal curve fits, primary and secondary feature time constants were calculated as the time point at which 63.2% of the difference from the feature value (latency or amplitude) at the initial time point and the projected value after 2 minutes of stimulation. This time constant definition was chosen because the sigmoid used was similar to the modified exponential used to represent an RC circuit, which commonly use the 63.2% measure. Goodness of fit was also used to determine useful trials for each feature property (i.e. primary feature amplitudes and secondary feature latencies). Only trials with Model 1 curve fits with an $R^2$ of at least 0.7 were used for further analysis. Curve fit parameters and feature latencies were combined across subjects. When plotting the data, data from subject So was normalized to its mean and multiplied by the mean in subject Az's data to keep the two subjects on the same scale. N1 feature amplitudes were plotted as negatives of the feature value for ease of comparison.

### 3.3.8 Statistical analysis

Individual comparisons in ECAP primary feature amplitudes and secondary feature latencies between the start and end of stimulation were performed using the Wilcoxon signed rank test (MATLAB's *signrank*), with data points paired by stimulation amplitude, stimulation pulse width, and stimulation and recording electrode locations. Comparisons of ECAP secondary feature latencies across changes in stimulation amplitude were first assessed for significant differences using a Kruskal-Wallis test

(MATLAB's *kruskalwallis* function). After a significant result from this test, individual comparisons were made using the Wilcoxon signed rank test as above, corrected for multiple comparisons using the Holm method. Reported p values account for Holm correction.

## 3.4 Results

During the first 30 seconds following STN-DBS onset, the ECAP primary feature amplitudes for both the observed negative trough (N1) and positive peak (P1) decreased significantly (Wilcoxon signed rank, $p<0.001$) (**Fig. 3-3A,B**). These habituation effects were noted for stimulation targeting either the STN or the LF. At clinically-relevant amplitudes (87.5% of the side effect threshold), the total primary feature habituation was 8% for N1, and 14% for P1 (**Fig. 3-3C**). The actual amplitude reduction over the 30 sec stimulation duration was larger for N1, but the percentage change (calculated on a pair-wise basis between start and end values for each trial) was lower than that for P1 given the larger N1 amplitude at baseline. Additionally, the habituation effect for N1 and P1 was stronger for higher amplitude stimulation, but only the effect on N1 was statistically significant (Wilcoxon signed rank, $p<=0.029$).

In contrast to the ECAP primary features, the ECAP secondary features did not have a consistent change in amplitude over the initial 30 seconds of stimulation. However, the appearance of the ECAP secondary features was delayed within the interstimulus time window over the wash-in period of STN-DBS (**Fig. 3-4**). This change was greater in subject So, but both subjects showed a statistically significant effect (Wilcoxon signed rank, $p<0.001$). Additionally, the delay in secondary features occurred for all peaks and troughs present, but was more apparent in the secondary features occurring between 4-6 ms after the stimulus pulse.

The wash-in dynamics of the primary feature amplitudes were best fit to a decaying sigmoid function, while the wash-in dynamics of the secondary feature latency was best fit to a growing sigmoid function (**Fig. 3-5A-C**). Across all data analyzed, 38% of subject Az's data and 49% of subject So's data fit this model (i.e. Model 1), while only 11% and 17% had a better fit with the polar opposite (i.e. Model 2). Data that did not have a good fit (defined as $R^2<0.7$) with Model 1 was not further analyzed. The majority of data with no fit (51% of all fits in Az and 34% of all fits in So) was a result of a lack of detection of secondary features, as not all recording configurations had secondary

features present in a way that could be detected. Secondary feature latencies typically increased by about 0.5 ms over the course of 30 seconds of stimulation. Time constants for these functions were between 5 and 12 seconds on average, but could be as long as 20-25 seconds (**Fig. 3-5D**).

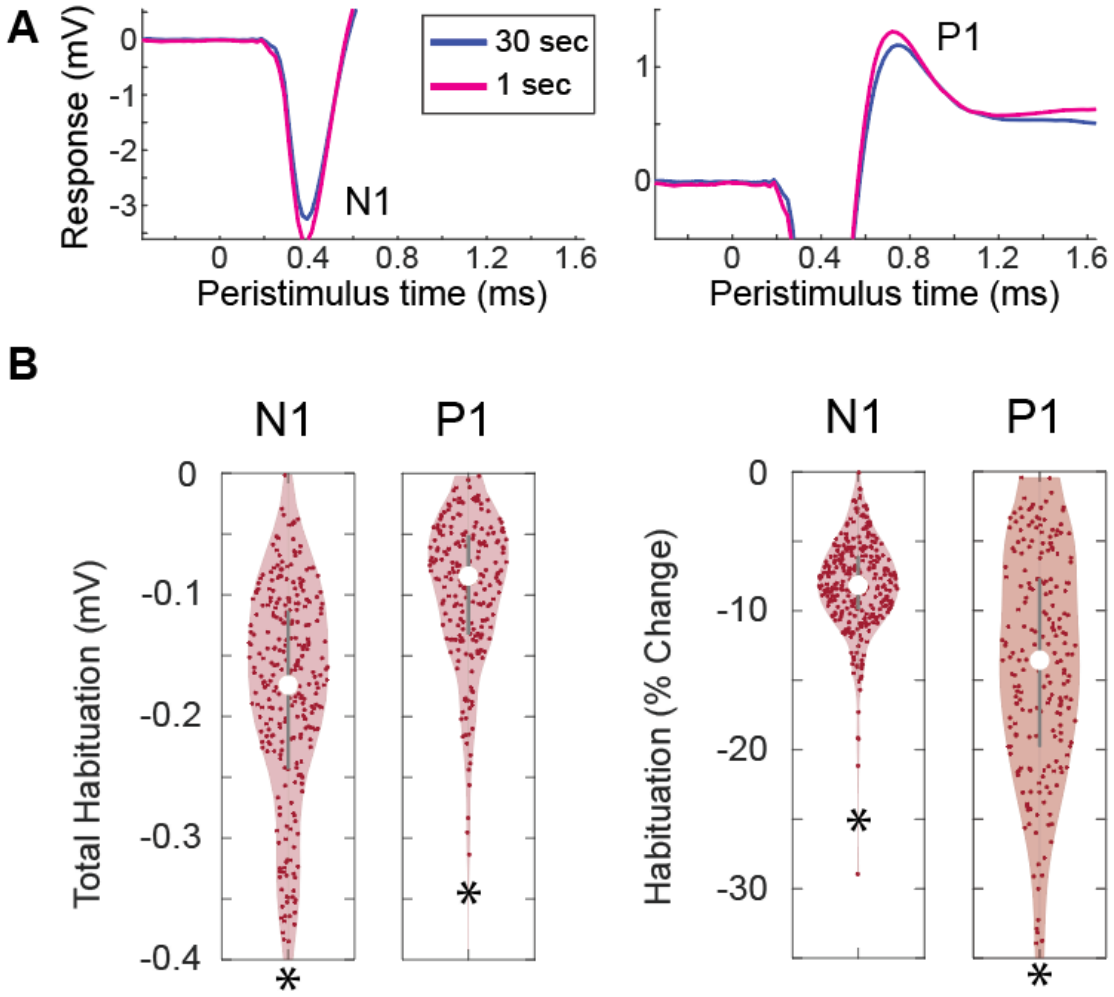


**Figure 3-3** Adaptation of ECAP primary features during STN-DBS. (A) Example primary feature recordings (P1 and N1) after 1 sec and 30 sec of stimulation. (B) Total amplitude reduction and the percent change in amplitude for all trials with stimulation at 87.5% of side effect threshold. All changes were significantly different from 0 ($p < 0.001$). Medians are shown as white dots.

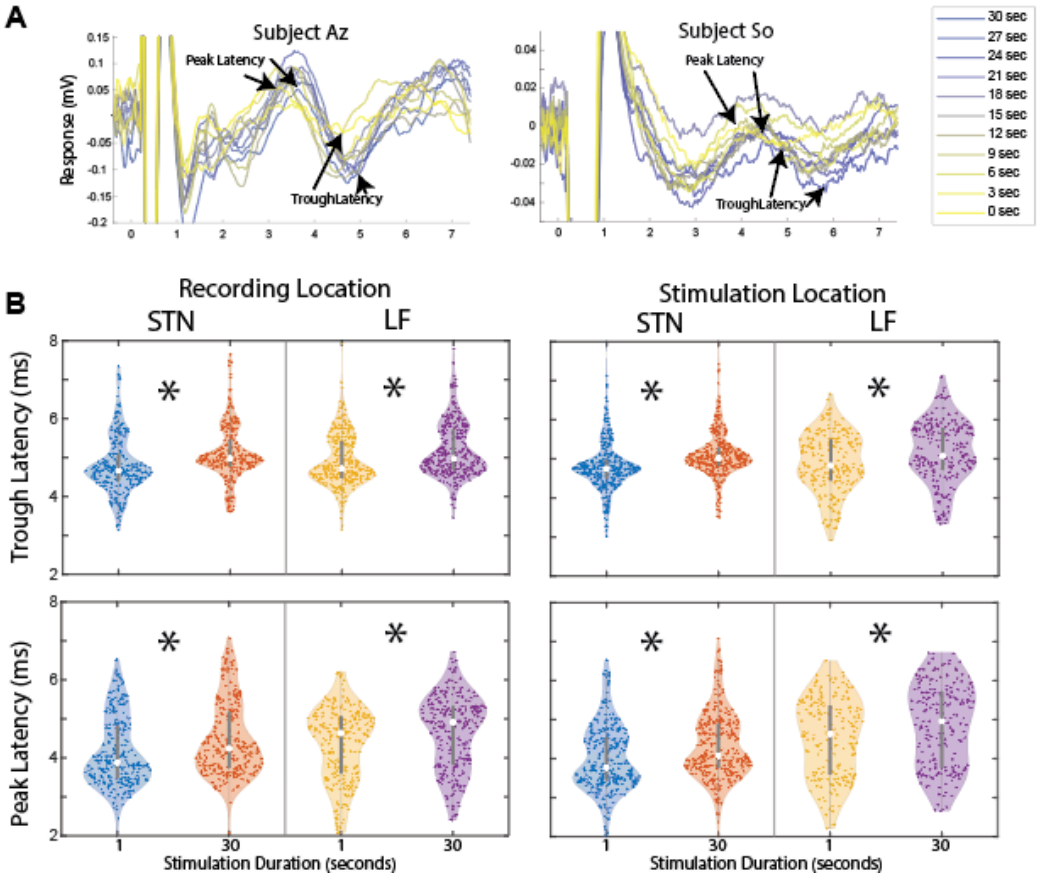


**Figure 3-4** Change in latency of ECAP secondary features during STN-DBS. (A) Example changes in ECAP secondary features over the course of 30 seconds of stimulation showing a temporal delay in feature appearance over time. (B) Violin plots showing the secondary feature latency change for the last peak and trough detected in each recording. Data is shown filtered by recording site or stimulation site, with each site containing data across all possible stimulation or recording sites and amplitudes. In all cases and for both features there is a significant latency shift from 1 second of stimulation to 30 seconds of stimulation. Feature latencies are drawn from the curve fits created from the measured latency data. Changes in latencies between 1 and 30 seconds of stimulation were all significant (all p values < 0.001). Medians are shown as white dots.

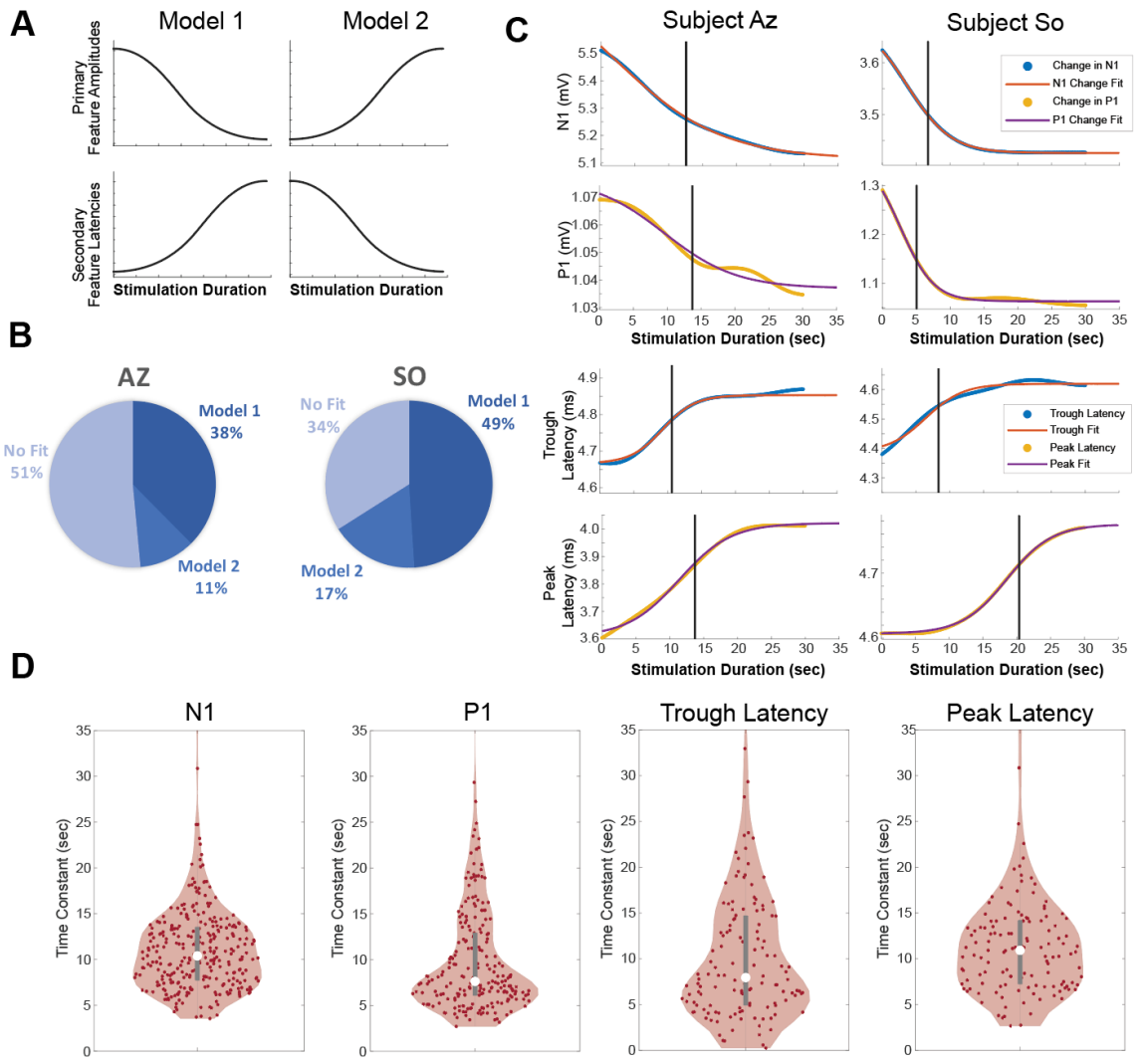


**Figure 3-5** Characterization of wash-in time constants for primary and secondary ECAP features. (A) Illustration of Model 1 and Model 2 sigmoidal dynamics for primary and secondary features. (B) Percent of data that best fit (i.e. $R^2 > 0.7$) between Model 1 and Model 2 for each subject. (C) Examples of curve fits using Model 1 for primary feature amplitudes and secondary feature latencies in both subjects. Vertical black lines indicate the time constant calculated for each curve fit. (D) Violin plots showing the time constants for primary feature amplitudes and secondary feature latencies at 87.5% of side effect threshold. Plots contain data across all stimulation pulse widths, stimulation sites, and recording sites. Medians are shown as white dots.

Although no consistent significant changes were observed in individual comparisons of secondary feature latencies with increasing stimulation amplitudes, both initial and end-of-stimulation latencies trended earlier with increasing stimulation amplitudes, with a total change of roughly 1 ms (**Fig. 3-6**). A Kruskal-Wallis test across starting latencies and ending latencies for each feature was significant ($p < 0.001$). Additionally, all location combinations (DBS targeting the STN or LF) had significant increases in latency over the course of 30 seconds of stimulation.

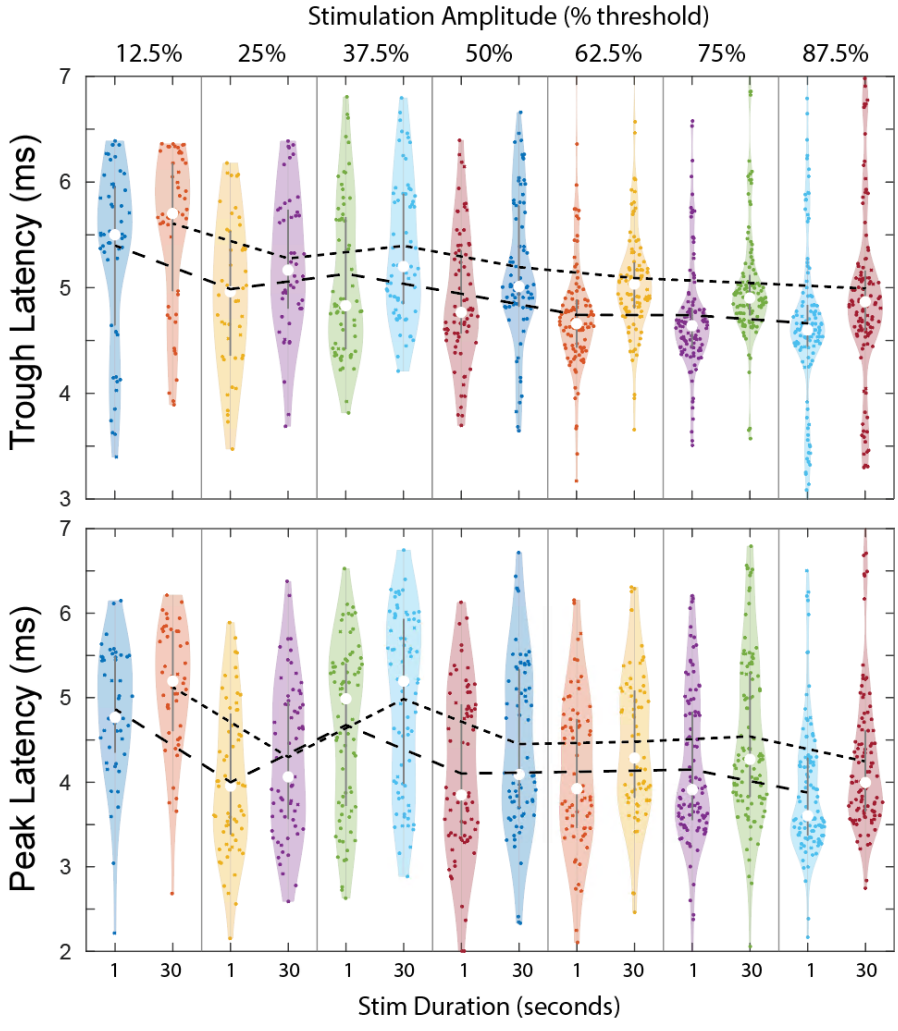


**0**

**Figure 3-6** ECAP secondary feature latencies by stimulation amplitude. Violin plots showing secondary feature latencies at the start and end of stimulation for each DBS amplitude tested. Data are shown across all possible stimulation or recording sites and pulse widths tested. Medians are marked with white dots. Black lines mark means, with broadly dashed lines connecting mean latencies after 1 sec of stimulation at each amplitude, and finely dashed lines connecting mean latencies after 30 sec of stimulation.

Change in secondary peak latencies tended to increase with increased stimulation amplitude when examined over all recordings, but separating the data into LF/LF and STN/STN stimulation/record configuration trials revealed differences in latency changes based on stimulation and recording site location (**Fig. 3-7**). LF/LF configurations had a decrease in latency change after one step in stimulation amplitude followed by no change with further increases to stimulation amplitude. In contrast, STN/STN configurations generated an increased latency of secondary features with increasing stimulation amplitudes (**Fig. 3-7B**). Despite some observed increases in secondary feature amplitudes (**Fig. 3-7A**), these changes were not consistent across recordings (**Fig. 3-4 A**),

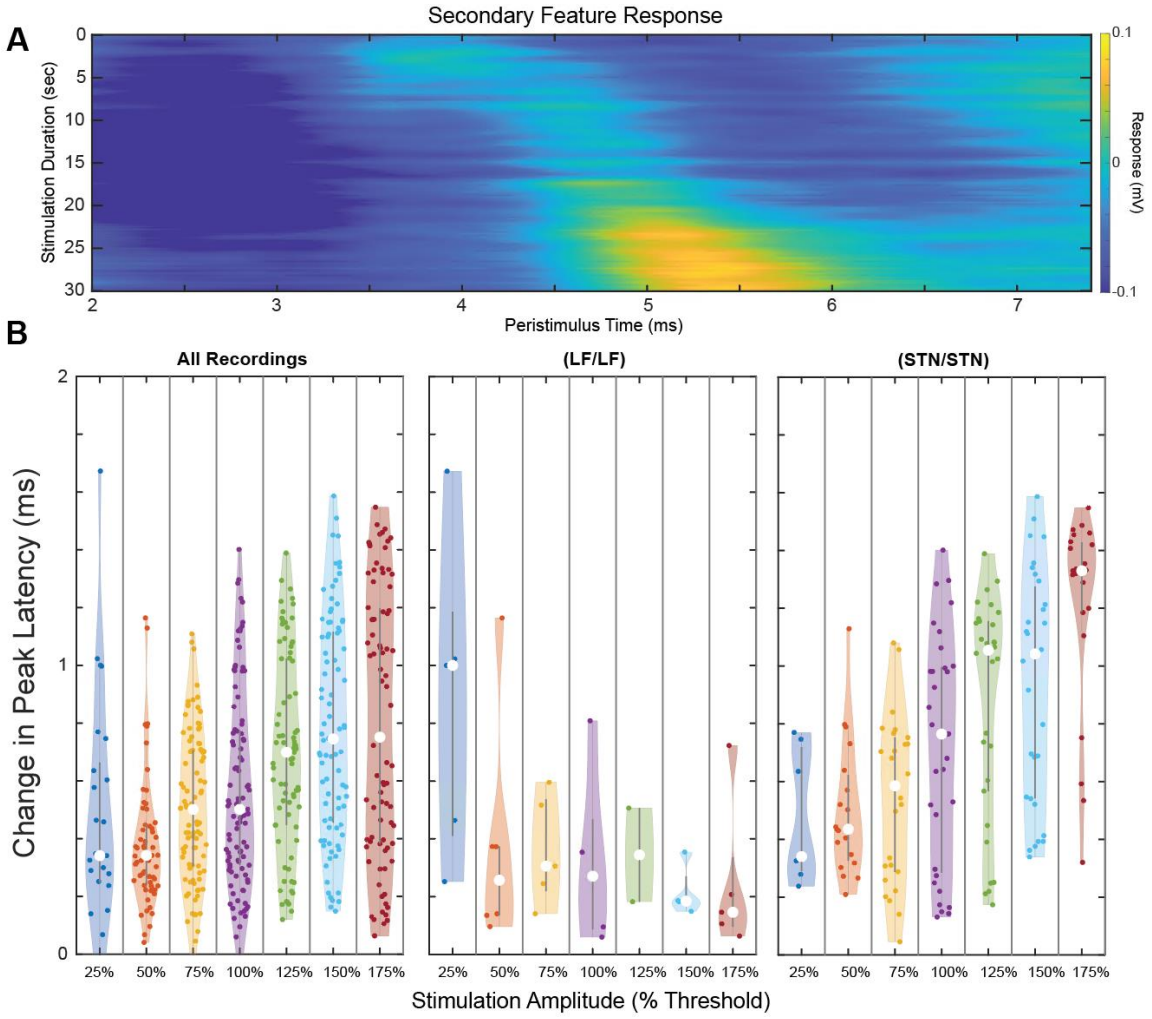


**Figure 3-7** Secondary features at stimulation amplitudes above side-effect threshold. (A) Example plot of secondary feature response over 30 seconds of stimulation showing changes in latency for secondary peak and trough features. (B) Violin plots showing the change in secondary peak latency over the course of 30 seconds of stimulation as it relates to stimulation amplitude for higher-amplitude trials for all stimulation and recording sites, LF/LF stimulation/record sites, and STN/STN stimulation/record sites.

## 3.5 Discussion

In this study, we investigated the temporal dynamics of ECAP features within the STN and LF during STN-DBS. Primary features habituated in amplitude over the course of the initial 30 seconds of stimulation, while secondary feature latencies increased by about 0.5 ms over the same time period, with changes of up to 1.5 ms possible with stimulation amplitudes exceeding the side-effect threshold for dyskinesias. Secondary

feature latencies in the STN trended toward greater increases in latency over the course of the initial 30 seconds of stimulation during STN-DBS with increasing stimulation amplitudes. Secondary feature latencies in the LF, on the other hand, had very little change with increases in stimulation amplitude. Previous studies have shown a similar pattern in the phase-locking of globus pallidus spike activity during STN-DBS [73,82], which may stem from, or result in, the direct neural modulation patterns observed in the present study as the globus pallidus has both efferent and afferent connections with the STN. This provides further evidence that STN and LF ECAP secondary features are a result of post-synaptic axonal activation of neurons that are part of the STN/globus pallidus network [50].

ECAP primary feature habituation may stem from a loss of synchronous axonal capture with each stimulus pulse, a reduction in excitability as a result of increased extracellular potassium concentrations with repeated axonal activation [83], or a reduction in action potential amplitudes over time. In fact, a reduction in the volume of activation of neuron populations has been observed during cortical stimulation in which the neurons active at onset of stimulation and at steady-state during high-frequency stimulation were spatially distinct [84]. Increases in extracellular potassium would result in lowered excitability and an increased likelihood of failure to generate action potentials or to allow action potentials to conduct along a given axon. Reduction in action potential amplitude with stimulation has been shown to occur in mammalian axons during high-frequency stimulation. However, this change occurs within one second of stimulation onset rather than the 5-10 second wash-in observed in this study [85,86], reducing the overall likelihood of action potential amplitude reduction being the explanation for primary feature habituation. Additionally, decreases in pre-synaptic action potential amplitude was also linked to reduction in synaptic latency, which further reduces the likelihood that changes in ECAP primary feature amplitude are due to a reduction in action potential amplitude [92]. Finally, A habituation in phase-locking over the first minute of stimulation was observed in a previous study examining the downstream effects of STN-DBS on spike activity in the globus pallidus [73], suggesting that there may be a loss of action potentials being generated in STN to globus pallidus connections during STN-DBS.

ECAP secondary feature responses, on the other hand, are thought to result from post-synaptic activity given their longer latency and the ability for pharmacological blockage of synaptic transmission to turn off the response [52]. The STN is intricately

connected with both segments of the globus pallidus [87], and likewise, the external globus pallidus projects back to the STN. Additionally, similar secondary ECAP feature latency changes were observed in the globus pallidus during STN-DBS [50], and the increase in secondary feature latencies align well with previously observed increased latency of neuron phase-locking in response to STN stimulation [73,82]. A later shift in these latencies indicates a slowing of the network, which may struggle to keep up with the same pace of high-frequency stimulation, especially at glutamatergic synapses [73]. Changes in feature latency could also be caused by a slowing conduction velocity from synaptic depression, or changes in presynaptic axon properties like increased extracellular potassium concentrations from axonal activation [88]. Changes at a synaptic level could be mediated by connections between the STN and the globus pallidus given that STN somatic activity is significantly attenuated during the period of secondary ECAP features with STN-DBS [82]. Similarly, synaptic depression has been shown to be more pronounced in cortical excitatory synapses [89], and STN connections to the globus pallidus are known to be excitatory in nature. Synaptic depression has also been shown to lead to changes in the phase of post-synaptic activity relative to a non-depressed state [90], and these changes have been seen to occur with time constants similar to those observed in this study [91]. Axonal contributions to changes in ECAP secondary feature latencies could consist of changes in conduction velocity in STN efferents to the globus pallidus as the change in latency mirrors the changes seen in globus pallidus somatic activity during STN-DBS [73,82]. Additionally, inhibition of pre-synaptic D-type (Kv1) voltage-gated potassium channels and shifts in pre-synaptic calcium currents have been shown to prolong the duration of the pre-synaptic action potential, which in turn increases post-synaptic response latency by up to 2 ms [92], and these channels are known to be present in STN neurons [93].

Decreased latencies of higher amplitude stimulation was inconsistent with results of a study linking ECAP responses to therapeutic outcomes [51]. However, the previous study used a bipolar recording configuration, which may have contributed to differences in the dipoles recorded within the ECAP signals. Additionally, in that study, stimulation was only delivered for 5 seconds, which may have led to differences in wash-in of the ECAP response. The fact that ECAP secondary feature latencies do consistently grow with time, however, fits well with the prior observation that later secondary feature latencies corresponded to better therapeutic outcomes at higher stimulation amplitudes.

This further supports a potential link between STN ECAP response wash-in and wash-in of STN-DBS therapy.

### 3.5.1 Limitations

This study and most previous studies on ECAP feature properties [50,51,54,64] have relied on specific feature detection using peak and trough amplitude and latency as the ECAP feature. However, spatial heterogeneity in ECAP responses (Chapter 2) was shown to necessitate the use of signal-agnostic feature detection for more objective analysis in order to compare signals with different feature latencies and numbers of features. Additional signal-agnostic methods should be developed to provide more broadly-applicable data analyses and reduce subjectivity in data analysis. Use of the *findpeaks* feature detection method in this study was done to improve comparability with previous studies and in the absence of a better method of measuring feature latencies. However, roughly 40-50% of all trials lacked sufficient feature detection using *findpeaks* to perform analysis (**Fig. 3-5B**) despite using a 0.8 second moving window to reduce noise at the cost of some temporal resolution in the stimulation duration axis. Studies analyzing wash-in of therapeutic effects typically record their measurements in timescales of multiple minutes, which does not allow for easy comparison of ECAP response changes to wash-in of therapy. However, the fact that the change typically happens between onset of stimulation and the first measurement time after stimulation onset does improve the likelihood of a link between ECAP feature changes and therapy wash-in, at least compared to an instantaneous change as happens with beta power during stimulation [81,94,95]. Stimulation amplitudes used in this study were dependent on side effect threshold, which lack the specificity of consistent stimulation amplitudes. However, this definition of stimulation amplitude does match clinical programming of stimulation amplitudes, which are often set as a percentage of side effect threshold. Finally, while this study used a sigmoid to model ECAP feature wash-in dynamics, there were some curves observed that may have also had damped oscillator dynamics, which could warrant the use of a different model than a sigmoid.

## 3.6 Conclusion

ECAP responses to STN-DBS are dependent on stimulation amplitude, stimulation location, and recording location, and change over the course of stimulation

with primary ECAP features habituating and secondary features increasing in latency. Primary feature habituation is suggested to be a result of axonal firing pattern entrainment or fatigue, while secondary feature latency increases suggest changes in circuit-level synaptic strength or axonal conduction velocity in the STN / globus pallidus network. In comparison to biomarkers of STN-DBS that change immediately with stimulation onset, the observed longer duration wash-in effects of primary and secondary ECAPs within and adjacent to the STN warrant further study to investigate possible links between STN ECAP dynamics and clinical wash-in of STN-DBS therapy.

# Chapter 4: Preclinical evaluation of a novel LCP-based deep brain stimulation electrode array: high-density deep brain recordings.

Adapted from work to be submitted to Transactions on Biomedical Engineering, “Deep Brain Stimulation Arrays with Liquid Crystal Polymer Substrates for Bidirectional Interfacing”

## 4.1 Chapter Overview

High-density deep brain electrode arrays have potential to significantly increase the feature space for clinician-programmed and adaptive deep brain stimulation (DBS) therapies. Previous DBS arrays have used polyimide substrates wrapped around a carrier lead. In this study, we report on development and evaluation of a DBS array with a thermoplastic-based liquid crystal polymer (LCP) substrate. Deep brain LCP arrays were fabricated with 48 (12 rows x 4 columns) electrodes, each coated with a rough platinum layer to increase charge-storage capacity, and then implanted in two parkinsonian non-human primates. Evaluation included resting-state local field potentials (LFPs), electrically evoked compound action potentials (ECAPs), and electrochemical impedance spectroscopy. Both chronically implanted DBS arrays retained the majority of viable electrodes after ~1 year of implantation and impedance magnitudes did not significantly change between pre-implant and post-explant measurements. Additionally, the DBS arrays showed spatial heterogeneity of LFP and ECAP features that were lost when recordings were analyzed in a 'ring'-mode configuration. LCP-based DBS arrays are capable of maintaining long-term bidirectional interfaces. LCP substrate technology paired with innovative site coatings allows higher amplitude stimulation, recording of heterogeneous neural signals, and good resiliency of leads during chronic implantation.

## 4.2 Introduction

Deep brain stimulation is an implantable therapy used to treat a variety of brain disorders [96]. While effective, the potential for inducing side effects with DBS therapy has resulted in innovation in the implanted electrode lead design, including the use of three split-band electrodes around the lead's circumference [97,98]. In such cases, if a lead is implanted slightly off-target, the split-band design allows one to better steer current away from pathways that induce side effects when stimulated [99,100]. Recent efforts to develop higher-density deep brain electrode arrays have shown promise in expanding the parameter space for steering electric fields around the lead [101] as well as improving the spatial resolution of local field potential recordings [102]. To date, these arrays have relied on a polymer substrate composed of polyimide, which can be prone to delamination and loss of substrate integrity [103].

Liquid crystal polymer technology has shown promising results with long-term *in*

*vivo* implantations, where µECoG arrays remained implanted for 3.4 years with stable impedance measurements [103]. As a substrate, LCP is flexible, durable, and is considerably more reliable than polyimide in salt spray, high humidity, and high temperature tests [104], all of which are valuable properties for chronic brain implant devices. Additionally, LCP is a thermoplastic, which enables thermal reshaping and resetting of internal stresses within the material when wrapping around a carrier tube for deep brain lead applications. When creating such electrode arrays with smaller geometric surface area sites, delivering high-amplitude currents without causing electrode corrosion can be challenging [105]. Previous studies have used site coatings including electroplated platinum [106], machine-lasered platinum [107], and conductive polymers [108] to increase the effective surface area of the electrodes.

In this study, we report on a high-density deep brain electrode array using an LCP substrate that is thermally reformed around a carrier tube to withstand chronic implantation and designed with rough platinum electrode coatings to enable higher stimulation amplitudes. Two leads were chronically implanted and one lead was acutely implanted in the globus pallidus (GP) of two parkinsonian non-human primates. Before implantation and after explantation chronically implanted electrodes were assessed for impedances, and the ability to record neural signals and provide safe stimulation were assessed *in vivo* post-implantation for both chronic and acute implantations.

# 4.3 Materials and Methods

## 4.3.1 LCP array design and fabrication

An LCP array was designed and developed with 48-channels for stimulating and recording from deep brain regions in non-human primates (rhesus macaques) (Fig. 4-1). Fabrication of the LCP (Dycoplast) arrays was performed by Dyconex AG (MST Company, Bassersdorf, Switzerland). The array design incorporated two embedded copper trace layers that were insulated by laminated LCP cover layers. Each LCP layer had a 25 µm thickness creating a flexible printed circuit (FPC) stack that was 75 µm thick. Trace width was set at 25 µm with 25 µm edge-to-edge spacing between traces and at least 125 µm spacing between the trace edge to the substrate edge.

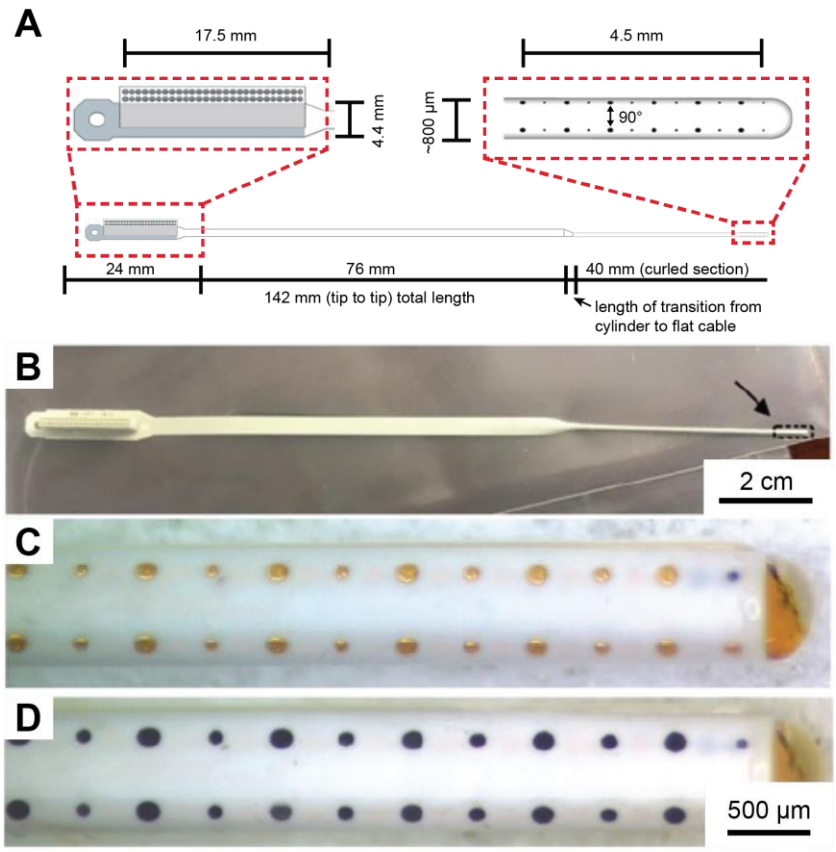


**Figure 4-1** High density DBS array components. Diagram (A) and picture (B) of the 48-channel LCP array and proximal connector. The curled lead tip before (C) and after (D) platinum electroplating.

The distal 4.5 mm end of the array was patterned with 12 rows each separated by 410 µm and each containing 4 contacts (alternating rows of 50 and 100 µm diameter electrodes). Electrodes on the surface of the cover layer were connected through 40 µm diameter vias to one of the trace layers. A thin layer of palladium followed by electroplated gold was used to coat the copper traces at each via. The distal portion of the LCP FPC was then wrapped around a rigid carrier tube and thermally reshaped creating a DBS lead body diameter of approximately 800 µm and a lead body length of 40 mm, which included the 4.5 mm lead body tip.

Traces from each electrode were routed through the flat portion of the flexible cable for several centimeters and bonded through via holes to a single nano-strip connector (Omnetics, Minneapolis, MN). This design provided physical separation between the lead body implanted within the brain and the externalized electrical pins of the connector. The FPC was designed to facilitate large batch production and each

section of the lead was designed to be adaptable to interfacing with several deep brain structures.

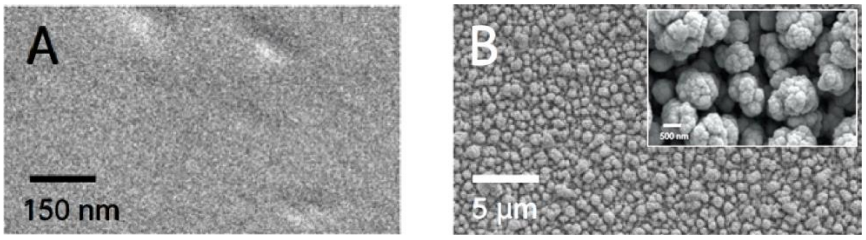


**Figure 4-2** High density DBS array coating. SEM of (A) bare platinum and (B) EPIC plated on a planar surface. EPIC coating greatly increased the surface area compared to platinum.

### 4.3.2 Platinum electroplating

The gold-surface electrodes underwent an electrodeposited platinum-iridium coating (EPIC) process using the procedures outlined in previous studies [109,110] to create electrodes with a high-surface area and increased charge storage capacity (Fig. 4-2). Briefly, the EPIC film was created by cycling an applied potential between an electrode on the LCP array and an Ag/AgCl electrode in a solution of 0.2 g/L of sodium hexachloroiridate (III) hydrate and 0.186 g/L sodium hexachloroplatinate (IV) hexahydrate in 0.1 M nitric acid. A small fraction of electrodes on the implanted arrays had a limited Pt-Ir coating because no electrodeposited gold site was present (see Fig. 4-1C at the distal lead tip showing the hypointense electrode site). Following the electrodeposition process, the resulting DBS arrays with LCP substrate and EPIC site material were sterilized using ethylene oxide gas (Anprolene EtO Gas Sterilizer).

### 4.3.3 Surgical procedures

Two parkinsonian non-human primates (*macaca mulatta*, subject Ga, 16 years, female; and subject Az, 18.5 years, female) were used to evaluate the performance of the DBS arrays *in vivo*. Each animal was imaged on a 7T or 10.5T MRI scanner with a custom-designed head coil for non-human primate brain imaging. These pre-operative images were used to plan the implant trajectory of each DBS array using a neurosurgical navigation software package (Preclinical Cicerone, contact the corresponding author for a copy). Subjects were instrumented with chambers oriented in an oblique anterior-to-

posterior and lateral-to-medial trajectory consistent with DBS lead implants targeting the globus pallidus in humans.

DBS arrays were implanted in the globus pallidus of both subjects (chronic, bilateral implant in subject Ga and acute, unilateral implant in subject Az). All DBS array implants were preceded by electrophysiological mapping of globus pallidus boundaries and functional territories using glass-tipped platinum microelectrodes (250 µm shank diameter, 0.8-1.2 MΩ, FHC) via the implanted DBS chambers. The DBS arrays were implanted using a stiff stylet at the center of the lead fed into a microdrive (Narishige, Amityville, NY) to drive the lead to the intended target. In subject Ga, each array was anchored to a ring within its DBS chamber, and the flex cables from each array were tunneled into another headcap chamber that housed both Omnetics connectors.

### 4.3.4 MPTP treatment

Both subjects were rendered parkinsonian with systemic injections of the neurotoxin MPTP (1-methyl-4-phenyl-1,2,3,6-tetrahydropyridine) consistent with previous studies [16], [17].

Following MPTP treatment, parkinsonian motor sign severity was rated for each subject using a modified version of the Unified Parkinson's Disease Rating Scale, consisting of 14 motor scores, quantified from 0 (no effect) to 3 (severe) (Imbert et al., 2000). The total motor score (max: 42) for each subject was used to determine the overall severity of parkinsonian motor signs. Averaged scores were 8.5 for Subject Az (mild), and 16.2 for Subject Ga (moderate).

### 4.3.5 Electrochemical impedance measurements

Electrochemical impedance spectroscopy measurements were performed prior to implantation and after explantation using a Metrohm Autolab potentiostat with sinusoidal waves ranging on a log-scale frequency from 0.5 Hz to 1 MHz with 10 samples per decade. These measurements were conducted in a solution of 1X PBS with an Ag/AgCl reference electrode. Impedances were analyzed with equivalent circuit analysis using *ZFit* for MATLAB [111]. The circuit model was kept simple with a single spreading resistance and constant phase element in series to represent the electrode interface pre-implant and post-explant. Changes in equivalent circuit model parameters were tested for significance using a paired t-test ($p<0.05$).

### 4.3.6 Resting state LFP recordings

Resting state LFP recordings from each DBS array electrode were sampled a 48.8 kHz using a PZ5 amplifier (Tucker Davis Technologies, Alachua, FL). The signals were passed through a 60 Hz notch filter, and then common average referenced using the mean of all viable channels. Spectral power of the LFP signals was calculated using MATLAB's *pwelch* function, converted to dB, and then normalized to the maximum power in the signal (typically around 0-1 Hz) for each channel. To remove 1/f noise, the spectral power at each electrode in the 0-10 Hz, 35-55 Hz, and 65-115 Hz bands was fit to a $1/f^{\alpha}$ curve, and this curve was subtracted from the channel's normalized power. $1/f^{\alpha}$ curve fits had adjusted $R^2$ values averaging 0.85 for subject Ga (left), 0.71 for subject Ga (right), and 0.89 for subject Az. The resulting data was then examined for beta band power in the low (15-20 Hz), and high (20-35 Hz) beta bands, with each band's power being normalized again by subtracting the maximum power in that band across all channels analyzed (setting maximum power to 0). Simulated row spectral power was calculated using the average of the recorded LFPs from the electrodes in the simulated row after removing the common average reference. This analysis was performed using 1 minute of data taken from a resting state recording.

### 4.3.7 ECAP recordings

Electrical stimulus pulse trains were delivered at 125 Hz through a single contact using charge-balanced biphasic pulse waveforms that alternated between cathodic- and anodic-leading polarities. The first phase had a duration of 100 μs with larger stimulus amplitude, while the second phase had a 1 ms duration with a lower stimulus amplitude. Using these stimulus parameters, amplitude thresholds for inducing side effects (e.g. muscle contractions or dyskinesias) were determined by increasing the overall stimulus amplitude until a sustained side effect was observed on the contralateral side. Following the determination of side effect thresholds for each electrode configuration, subsequent stimulation trials were capped at 25 μA below the corresponding side effect threshold for that electrode on the DBS array. Stimulation was delivered for 20 seconds at a time.

ECAP responses were calculated from alternating polarity stimulation trials. First, baseline subtraction was applied to each interstimulus segment (8-ms long) by subtracting the signal amplitude at 0.35 ms before the stimulus pulse from all subsequent data points in the interstimulus segment. Next, segments were sorted based

on cathodic-anodic or anodic-cathodic stimulus waveforms to ensure that the sample sizes for both stimulus waveforms were identical. All ECAP responses over the last 20 sec of stimulation at a given electrode were averaged together. The resulting data were then smoothed (4-sample moving average over the first 1.17 ms and 16 sample moving average over the remaining portion of the segment). This two-part filtering approach avoided over-smoothing the primary features while still removing high frequency noise from the secondary features of the ECAP.

## 4.4 Results

The total coated, viable electrodes on each chronically implanted DBS array remained high after 1 year, with a total loss of 6 out of 85 electrodes across both leads, or roughly 7% (Fig. 4-3A). The left hemisphere DBS array began with 2 open channels and ended with 4, while the right hemisphere array began with 1 and ended with 5. Equivalent circuit analysis of the impedance spectroscopy measurements taken from a subset of coated, viable electrodes before implantation and after explantation showed a significant increase in interface capacitance (α parameter increased from 0.7 to 0.9, $p<0.001$), while the impedance magnitude showed no significant change (mean K parameter remained the same, $p=0.063$) (Fig. 4-3B,C).

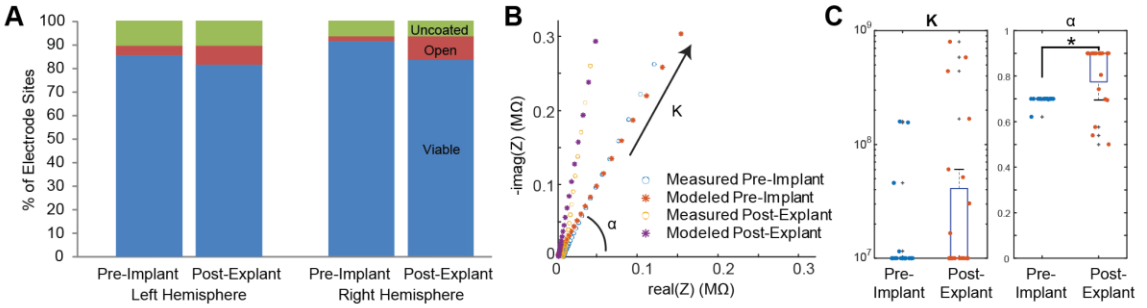


**Figure 4-3** Impedance analysis of implanted site coatings. (A) Plots showing percentage of viable, coated channels at implant and after explant of each DBS array. (B) Equivalent circuit model analysis of impedance data showing the Nyquist plot slope increased from pre-implant to post-explant. (C) Parameters K and α fits from electrical circuit analysis model from pre-implant and post-explant impedance measurements.

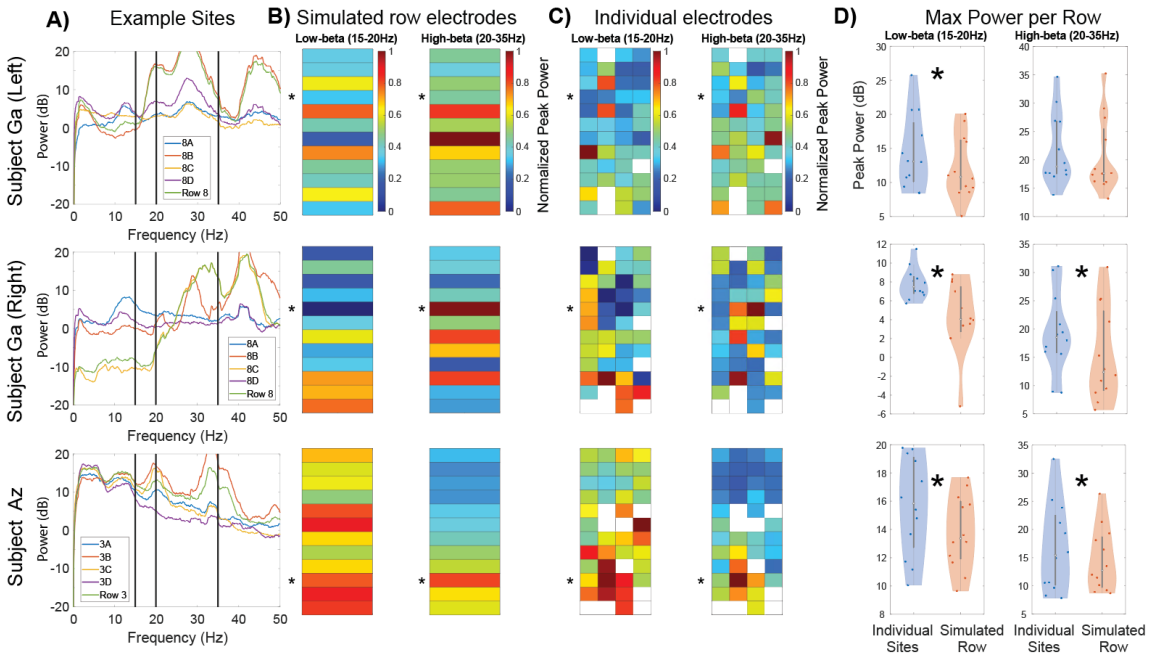


**Figure 4-4** Resting state LFP recording heterogeneity. (A) Example power spectra from a row of electrodes for each DBS array showing differences between single electrode and grouped row configurations. (B) Heat maps showing the normalized low and high beta power as recorded from simulated row electrodes. (C) Heat maps of the data from part B, but across all individual electrodes. Channels with higher noise or which were known to be open circuits are marked in white. (D) Violin plots comparing maximum peak beta power across individual electrodes from each row with the peak beta power recorded in the simulated row. Maximum recorded peak low beta power was significantly greater in individual electrode recordings than simulated row recordings ($p < 0.05$, paired T-test). In most cases maximum recorded peak high beta power was significantly different from that recorded in simulated rows ($p < 0.05$, paired T-test). Asterisks in B and C indicate the row of channels shown in part A.

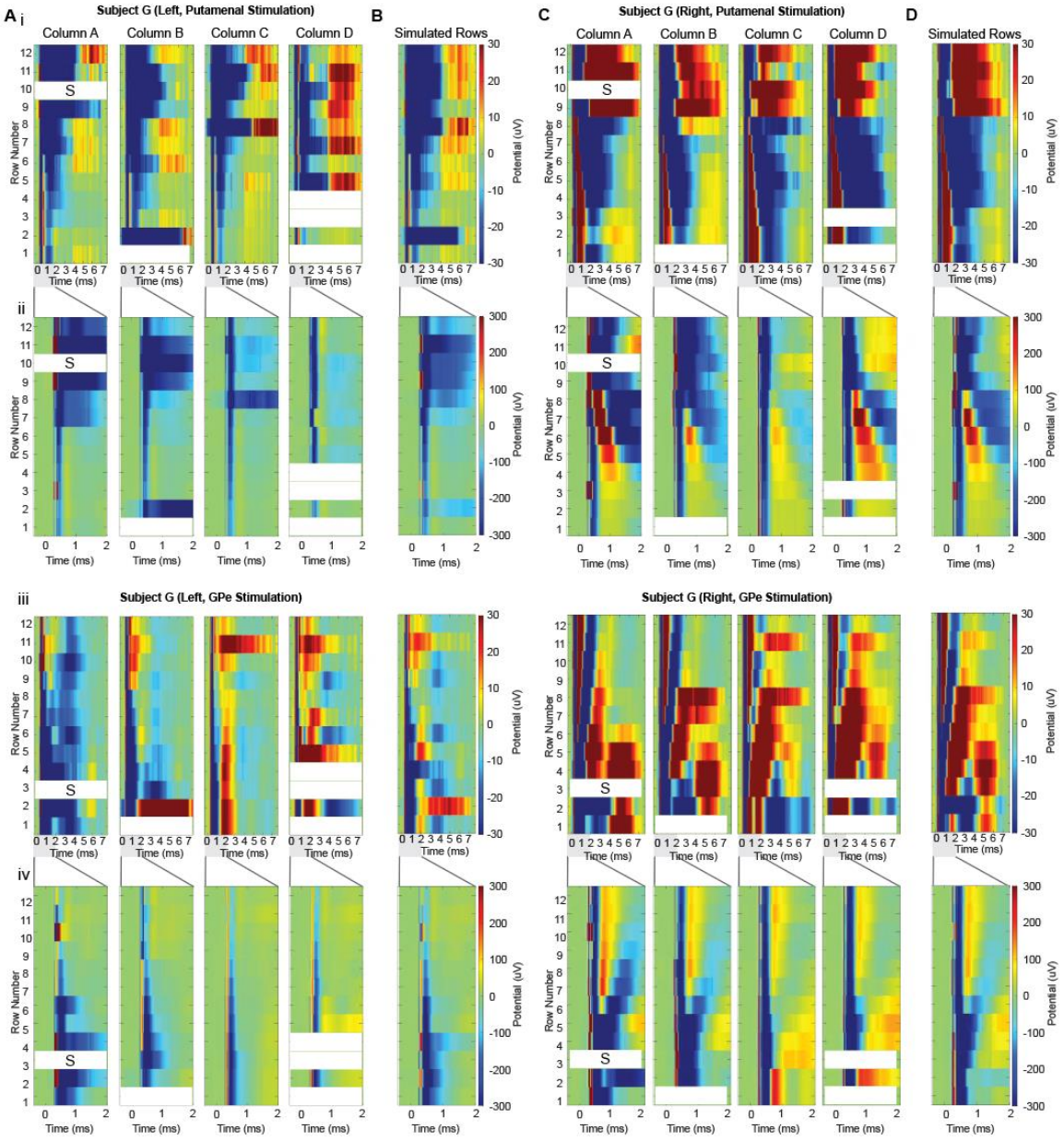


**Figure 4-5** ECAP heterogeneity in GPe and putamenal stimulation. Monopolar ECAP responses across all sites (A and C) or simulated row (B and D) to stimulation targeting the putamen (top row) or GPe (bottom row). Parts i and iii show full ECAP response, while parts ii and iv show a zoom of first 2 ms of the ECAP response, with color scale range increased 10-fold to show the full spectrum of values in the early ECAP response. White bars indicate open channels, with an S marking the stimulation site.

To study the heterogeneity of resting state LFPs, beta band power was compared between columns and rows on all three DBS arrays (Fig. 4-4A). When electrodes were grouped into rows, there was a clear loss of spatial information on beta band power (Fig. 4-4B,C). In some cases, electrodes recording large beta band power were lost in the average (Fig. 4-4A); conversely, other rows had a single channel dominate the row with an otherwise diverse set of signals (Fig. 4-4B,C). Additionally, the maximum beta power peak in a given row was significantly higher for low beta peaks when recorded through individual electrodes as compared to the simulated row recording (Fig. 4-4D)

DBS arrays were also able to evoke and capture ECAPs in response to stimulation (Fig. 4-5A,C). Appearance of evoked potentials depended on stimulation and recording locations, with the highest amplitude responses observed at sites closest to the stimulation site and ECAP wavefronts extending from those sources. Heterogeneity of responses was more readily visible when observed through individual electrodes (Fig. 4-5A,C) than through simulated row electrodes (Figure 4-5B,D).

## 4.5 Discussion

In this study, we report on the development and evaluation of a novel high-density DBS array using a thermally reshaped LCP substrate and microelectrodes coated with a rough platinum-iridium layer to increase their charge storage capacity. The majority of electrodes continued to be viable after ~1 years of implantation, and the DBS arrays showed more detailed spatial heterogeneity of LFP and ECAP responses than could be gleaned from macro-scale electrode contacts. Together, the arrays show promise towards providing higher density bidirectional interfacing for DBS therapy.

LCP as a substrate for bidirectional deep brain interfaces has several advantages. Most notably, the thermal shaping property enables bending the substrate and metal traces into a cylindrical form factor and then resetting the material stresses through heat. This obviates issues that other polymer substrates have with delamination between microfabricated layers [103]. LCP is also a material shown to hold up robustly in wet and corrosive environments, with minimal water absorption [104]. The LCP material has also been shown to have no harmful effects on tissue through biocompatibility testing [112].

The arrays were shown to enable bidirectional interfacing with deep brain structures. First, the heterogeneity of LFP beta power across the array matches a previous study's results from implantation of a high-density electrode array in the subthalamic nucleus of parkinsonian non-human primates [102]. Together, these studies show that many of the resting-state oscillatory dipoles within the globus pallidus and the subthalamic nucleus are of a finer spatial scale than what large macroelectrode contacts are able to detect given shunting of those sources. Similarly, the arrays were able to measure ECAP responses with features that depended on the stimulation target and that varied in time with some stimulation sites evoking spatially localized effects (Fig. 4-5A) and others evoking traveling waves (Fig. 4-5C).

Stimulation through the arrays and site coatings was able to be of a sufficient current amplitude to result in ECAP responses and testing of side effect thresholds without loss of any coated sites as a result of experimental stimulation. This suggests that the coating used for the electrodes was able to extend current densities beyond the traditional limits used for DBS leads with platinum-iridium, macro-scale electrodes. Smaller electrode sites present opportunities to deliver DBS therapy with less tissue damage through thinner diameter leads as well as potentially through implants with electrodes positioned in three-dimensional configurations to enable more advanced electric field orientations [113].

Several limitations should be considered in the interpretation of the study. First, the data from this proof-of-concept study was collected from a limited number of subjects and implants. Extending these *in vivo* results in the context of continuous DBS pulses applied over years through these microelectrode contacts will be important to evaluate the translational potential of the stimulation technology for human applications. Additionally, although there was no evidence of damage to the lead as a result of stimulation, we were unable to collect data about potential tissue damage with higher than normal charge densities. However, previous data suggests that the traditional charge density safety limits are much higher for micro-scale electrodes [114].

## 4.6 Conclusions

A novel high-density deep brain electrode array was developed and tested preclinically in acute and chronic implant preparations. The arrays showed stability in impedance over time, the ability to record LFPs and ECAPs with fine spatial selectivity,

and the capacity to deliver relatively high amplitude stimulation through microelectrode sites as small as 50 μm diameter without causing damage to the electrode. Overall, the arrays performed well and were capable of recording both resting state local field potentials and stimulation-evoked compound action potentials at a much finer spatial resolution than current directional DBS lead technology. We consider them an improvement over previous polyimide-based, high-density DBS arrays in terms of their longevity during chronic implantation.

# Chapter 5: Conclusions and Perspectives

## 5.1 Summary of Outcomes

In this thesis, the spatiotemporal characteristics of ECAP responses in and around DBS targets for treating the motor signs of Parkinson's disease were investigated in the context of stimulation amplitude, stimulation pulse width, and stimulation and recording location. ECAP feature amplitudes increased non-linearly with increases in stimulation amplitude, with a minimum stimulation amplitude required to evoke any response and a higher stimulation amplitude required to evoke secondary feature responses. Several of the results have important implications for future development of closed-loop DBS systems that seek to utilize ECAP features. First, the primary features of the local ECAP response during STN-DBS were most prominent when stimulating in the LF region dorsal to the STN. This feature provided strong separability in knowing which electrodes were dorsal to or within the STN, which can be helpful when programming STN-DBS implants. Second, both primary and secondary features adapt over the course of the initial thirty seconds following stimulation onset, which suggests habituation of local axonal capture by stimulation as well as delays in the basal ganglia circuit during STN-DBS. Third, while the directional DBS leads used in Chapters 2 and 3 provide a higher spatial resolution of ECAPs over all previous clinical ECAP studies with DBS applications, the electrodes sizes were still quite large relative to the anatomical target. We developed a high-density DBS array with microelectrodes to record even higher resolution ECAP activity, and tested this in the globus pallidus and putamen. The use of the liquid crystal polymer substrate resulted in stable impedances over the course of a year of implantation, making it a great improvement over previous polymer probe-based technologies.

### 5.1.1 Spatial heterogeneity of ECAPs in the STN: use of the ECAP in identifying implant location

In Chapter 2, a linear classifier was used to identify lead location between STN and LF regions, with ground truths drawn from block-faced imaging histology. Prior to analysis of the block-faced imaging, lead locations had been estimated entirely from pre- and post-operative imaging, which resulted in some incorrect depth estimations, trending toward an overestimation of implant depth (subjects Az and So were initially believed to be implanted one row deeper, with all stimulated sites placed in the STN). As evidenced with cross-subject classification (training the classifier on data from three subjects and

testing on a fourth), the classifier was able to accurately determine the brain region in which the electrodes were truly located, even without knowledge of any ground truths in that subject. This suggests that ECAP responses may be a useful complement to imaging procedures in determining implant depth in the STN region. This stemmed from a statistically significant change in ECAP response features (both in number of secondary features and amplitude of primary features) between STN and LF stimulation and recording, suggesting that the alignment of axons along the LF tract creates a stronger primary feature effect and the presence of neurons within the STN enables secondary features to appear. Other electrophysiological features have been proposed to identify electrode location within the sensorimotor STN, including mean beta power; however, the exact location of the recorded spectral features can vary by several millimeters, especially considering the necessity to use bipolar electrode montages [69]. ECAP features and beta oscillatory power may thus complement each other to identify locations of implanted DBS electrodes within a patient's STN.

### 5.1.2 Temporal changes in ECAP features: "wash-in" effect

ECAP responses from STN-DBS changed over the course of the initial thirty seconds of stimulation with primary features habituating in amplitude and secondary features increasing in latency. Primary feature habituation seems a likely result of loss of axonal capture, while secondary feature latency increases may result from changes in axonal conduction velocity and synaptic coupling in the STN / globus pallidus network. The time constants of these changes in both primary and secondary features at clinically-relevant stimulation amplitudes were about 5-12 seconds, which better aligns with the wash-in times seen in therapeutic stimulation than the instantaneous changes in beta band activity seen under similar stimulation conditions. Although the ability to test time constants over such short periods of time in therapeutic outcomes is extremely limited, therapeutic effect of stimulation is generally not instantaneous, instead commonly reaching a therapeutic state within 2-5 minutes – the first measured time point after onset of stimulation [81,94,95]. A previous study connecting STN ECAP response secondary features to therapeutic outcomes showed a later latency of secondary features in therapeutic trials [51]. The fact that secondary feature latencies grew over the duration of stimulation and that later secondary feature latencies corresponded to better therapeutic outcomes at higher stimulation amplitudes in the aforementioned study

suggests another possible link between STN ECAP feature wash-in and wash-in of STN-DBS therapy.

### 5.1.3 Use of LCP substrate in high-density DBS arrays and spatial heterogeneity of ECAPs and beta power in the GP and putamen

Use of high density arrays in the globus pallidus and putamen to record both LFP and ECAP responses revealed a high level of spatial heterogeneity in both signals. Heterogeneity in beta power matched with results from a previous study with a similar lead design implanted in the STN [102], and the heterogeneity visible in ECAP responses was visible with greater detail than could be seen in simulated row electrodes. Additionally, with 12 rows to record from, ECAP signals were seen to traverse the lead from top to bottom or bottom to top in a manner that resembled a traveling wave front, with primary features growing slightly wider, later in latency, and lower in amplitude as recording sites grew in distance from stimulation sites. Although the directional leads used in Chapter 2 and Chapter 3 did not typically have enough rows to observe this, the 8-row annular lead from subject Bl was also observed to have the phenomenon, as was another 8-row annular lead implanted in the thalamus of a subject not shown in any chapter (**Fig. 5-1**). Between the two 8-row DBS leads, the phenomenon was most clearly observable in the thalamus, and less distinct in the STN and its dorsal regions. This phenomenon, combined with the notion that ECAP features are a result of axonal activation, may potentially allow ECAP features to be used to assess local fiber tract activation around the lead if conduction velocities for those fibers are known. This is further supported by primary feature generation in Chapter 2 and Chapter 3 being the strongest in LF, which is a region with strongly aligned white matter fibers as compared to the STN which has more jumbled axon orientations. Additionally, the fact that the phenomenon applies to primary features alone rather than secondary features further supports the possibility that these traveling waves are a reflection of action potentials traveling along fibers oriented roughly parallel to the lead.

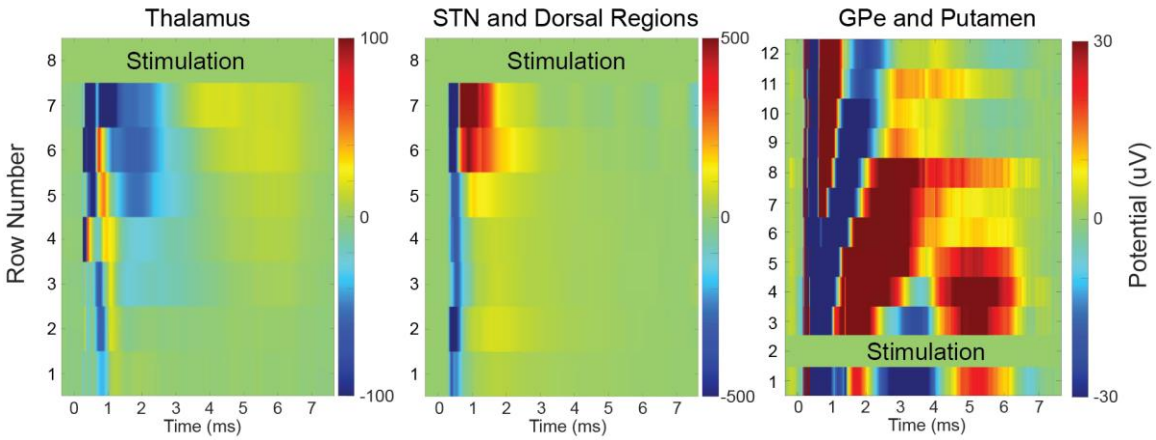


**Figure 5-1** ECAPs as traveling waves. ECAP responses in the motor thalamus, STN and its dorsal regions, and GPe and putamen with stimulation near one end of a DBS lead and recording from channels along the lead. ECAP primary features are seen to increase in latency and reduce in amplitude as the recording site moves farther from the stimulation site. Sites in GPe and putamen are simulated from a high-density array with 4 electrodes in each row averaged together to mimic a 12-row lead. Row numbers are ordered from most ventral to most dorsal.

### 5.1.4 Need or use for directional DBS leads

Interestingly, the results in Chapters 2 and 3 do not seem to indicate a strong dependency on directionality in ECAP response to stimulation in the STN and LF, while the signals recorded in the putamen and GP presented in Chapter 4 suggest a slightly higher degree of directional heterogeneity. It is possible that the directional leads used in Chapters 2 and 3 have electrodes that still short oscillatory dipoles and using a higher density array as in Chapter 4 in the STN could show stronger directional heterogeneity. Directional leads have been shown to be useful in improving targeting of stimulation and steering of electric fields, which can be especially helpful in avoiding side effects and in correcting for lateral errors in implant targeting [20,21]. Additionally, there may be cases where some electrodes within a row are in a different brain region than others on the same row. The ability to stimulate and record from separate directions can only improve the classification of lead depth by providing additional data points for the model to test or train on.

## 5.2 Future Directions

### 5.2.1 Signal-agnostic ECAP analysis methods

Deep brain stimulation technology is rapidly moving to incorporate higher density electrode arrays and recording feedback with more complex signals and more complex spatial combinations for stimulation and recording electrodes as seen in Chapter 4. With this movement, signal-agnostic and objective analysis methods become increasingly important – both for the sake of the consistency of measurements across research studies and for the sake of the researchers whose time will become exponentially more consumed with data analysis using traditional methods. For example, many older studies that some of the methods used in this thesis were based on used bipolar recording configurations with a single stimulation site, resulting in a single signal recorded per stimulation parameter tested in each subject. This may have resulted in 10-20 total signals – all of which were very similar to each other – within a given subject for perhaps a total of 100 signals if a study had 5-10 subjects and 10-20 tested parameters. On the other hand, conducting similar experiments as was done in this thesis work using directional DBS leads yielded 4900 different combinations in just two subjects (subjects Az and So in Chapter 2 and Chapter 3), with many unique signals across those various combinations. Furthermore, a high-density DBS array as was investigated in Chapter 4 could result in nearly 80,000 combinations from single-site stimulation in a single subject alone if tested in the same manner as was done in Chapter 2 and Chapter 3. As shown in Chapter 2, the use of summary statistics such as RMS values can greatly help in reducing the dimensionality of recorded signals while also making analysis more objective and signal-agnostic, as well as reducing the effects of noise on the outcome measure. Other such methods have also been recently proposed [115], and based on the results shown in Chapter 3, methods to determine a signal's duration and overall feature amplitudes as the signal itself changes may be helpful in further understanding the various characteristics of signals over the course of stimulation onset.

### 5.2.2 Clinical subject-agnostic ECAP classifier for lead depth

As shown in Chapter 2, a subject-agnostic classifier can be trained using ECAP responses recorded from a set of subjects and used to determine electrode depth in new subjects with good accuracy. As clinical DBS leads improve and gain the capacity for

signal recordings (like the Medtronic Percept devices), a wealth of ECAP signals should become available, not to mention any recordings that could be taken just before implantation of the stimulator (after lead implantation), that could be used to develop a highly accurate model for use in clinical patients. Currently, once a lead has been implanted there is no accurate electrophysiological measure for lead depth beyond what was assumed during implantation. Implant depth can be different from what was planned, and as leads grow in complexity clinicians will need to find ways to reduce programming time. Having a clinical tool for identifying electrode locations in brain regions around the STN could assist in reducing programming times by identifying electrodes most likely to produce therapeutic results.

### 5.2.3 Stimulation frequency analysis of ECAP responses

In this thesis, sweeps of amplitude, pulse width, and stimulation and recording location were tested, with ECAP response depending primarily on stimulation amplitude and stimulation and recording electrode location. Stimulation frequency, however, was not tested, in part because therapeutic DBS typically requires pulse train frequencies above 100 Hz. This leaves a gap in our understanding that may be useful to fill as stimulation therapies for other conditions may use different stimulation frequencies.

### 5.2.4 Relationship between ECAPs and evoked resonant neural activity

During the thesis work, some attempts to analyze the evoked resonant neural activity (ERNA) recorded alongside the ECAP responses were made, and observations that ECAP secondary features follow similar patterns to observed patterns in ERNAs were made [116,117]. However, no ERNAs were able to be detected from the data recorded in these experiments and that line of research was unable to be thoroughly explored. In particular, both ERNAs and STN ECAP secondary features seem likely to result from resonant activity within the STN / globus pallidus network, and this warrants research into similarities and differences between the two signals, particularly whether or not they are one and the same and how the ERNA response arises despite a lack of STN cell body activity during STN-DBS [82].

### 5.2.5 Challenges in making ECAPs clinically relevant

In order to record ECAPs in a clinical implant, improvements to implant technologies and clinical stimulation protocols are likely necessary. For example, the spectral components of ECAP responses in the STN can be as high as 2 kHz for primary features and as slow as 250 Hz for secondary features. This would necessitate at least a 4 kHz sampling rate to detect the primary feature waveform, or a minimum of a 500 Hz sampling rate for secondary feature detection. The Medtronic Percept device currently records at a sampling rate of 250 Hz, which is far too slow for the detection of primary ECAP features – the features that were most relevant to the classifier in determining lead implant location between STN and LF. The sample rate also plays a role in determining how consistent the stimulation artifact is between pulses, which in turn affects the recording accuracy of any features that may overlap with stimulation-induced noise.

Clinical DBS also uses passive recharge rather than active recharge in stimulation [118–120], resulting in potential differences in stimulation artifact, not to mention a reliance on cathodic-leading pulses, requiring a more complex stimulation artifact removal technique, such as the development and subtraction of an artifact model. Although the use of an adapting artifact model may be relatively simple to implement in a research lab, it likely requires more computational power than a simple average as can be used for alternating polarity stimulation. This could lead to increased power draws on the stimulator battery and place limitations on the device's internal memory.

Additional research on the therapeutic outcomes of alternating polarity stimulation could be warranted if ECAPs are to be used in a closed-loop setting, but simply making it possible in the device programming would allow clinicians to use this setting when using ECAPs to confirm lead location after implant. An alternative to alternating polarity stimulation is to lead with the long (low-amplitude) anodic phase and follow up with the short (high-amplitude) cathodic phase (the phase that would evoke the ECAP). This places the majority of the stimulation artifact at the end of the signal rather than the beginning, and reduces the overlap of artifact with primary feature signal (albeit at the cost of late secondary feature signal). Additionally, equiphasic stimulation could be used to reduce the duration of the recharge phase artifact. Finally, in this study there was very little change in ECAP response across different pulse widths tested. The use of

a narrower pulse width can increase side effect thresholds and allow the application of stimulation with even less overlap of stimulation artifact with ECAP response.

# Bibliography


[1] Tysnes O-B, Storstein A. Epidemiology of Parkinson's disease. J Neural Transm (Vienna) 2017;124:901–5. https://doi.org/10.1007/s00702-017-1686-y.

[2] Polymeropoulos MH, Lavedan C, Leroy E, Ide SE, Dehejia A, Dutra A, et al. Mutation in the alpha-synuclein gene identified in families with Parkinson's disease. Science 1997;276:2045–7. https://doi.org/10.1126/science.276.5321.2045.

[3] Erekat NS. Apoptosis and its Role in Parkinson's Disease. In: Stoker TB, Greenland JC, editors. Parkinson's Disease: Pathogenesis and Clinical Aspects, Brisbane (AU): Codon Publications; 2018.

[4] Parkinson's Disease: Causes, Symptoms, and Treatments. National Institute on Aging n.d. https://www.nia.nih.gov/health/parkinsons-disease (accessed September 20, 2022).

[5] Goetz CG, Fahn S, Martinez-Martin P, Poewe W, Sampaio C, Stebbins GT, et al. The MDS-sponsored Revision of the Unified Parkinson's Disease Rating Scale 2019:33.

[6] Koller WC, Rueda MG. Mechanism of action of dopaminergic agents in Parkinson's disease. Neurology 1998;50:S11–4. https://doi.org/10.1212/WNL.50.6_Suppl_6.S11.

[7] Deep Brain Stimulation | Parkinson's Disease n.d. https://www.michaeljfox.org/deep-brain-stimulation (accessed September 20, 2022).

[8] Bradykinesia (Slowness of Movement) | Parkinson's Foundation n.d. https://www.parkinson.org/understanding-parkinsons/symptoms/movement-symptoms/bradykinesia (accessed September 20, 2022).

[9] Tremor | Parkinson's Foundation n.d. https://www.parkinson.org/understanding-parkinsons/symptoms/movement-symptoms/tremor (accessed September 20, 2022).

[10] Rigidity | Parkinson's Foundation n.d. https://www.parkinson.org/understanding-parkinsons/symptoms/movement-symptoms/rigidity (accessed September 20, 2022).

[11] Aziz TZ, Peggs D, Agarwal E, Sambrook MA, Crossman AR. Subthalamic nucleotomy alleviates parkinsonism in the 1-methyl-4-phenyl-1,2,3,6-tetrahydropyridine (MPTP)-exposed primate. Br J Neurosurg 1992;6:575–82. https://doi.org/10.3109/02688699209002375.

[12] Bergman H, Wichmann T, DeLong MR. Reversal of experimental parkinsonism by lesions of the subthalamic nucleus. Science (New York, NY 1990;249:1436–8.

[13] Bratsos S, Karponis D, Saleh SN. Efficacy and Safety of Deep Brain Stimulation in the Treatment of Parkinson's Disease: A Systematic Review and Meta-analysis of Randomized Controlled Trials. Cureus n.d.;10:e3474. https://doi.org/10.7759/cureus.3474.

[14] Deep brain stimulation - Mayo Clinic n.d. https://www.mayoclinic.org/tests-procedures/deep-brain-stimulation/about/pac-20384562 (accessed September 20, 2022).

[15] Cyron D. Mental Side Effects of Deep Brain Stimulation (DBS) for Movement Disorders: The Futility of Denial. Frontiers in Integrative Neuroscience 2016;10.

[16] Zarzycki MZ, Domitrz I. Stimulation-induced side effects after deep brain stimulation – a systematic review. Acta Neuropsychiatrica 2020;32:57–64. https://doi.org/10.1017/neu.2019.35.
[17] Dallapiazza RF, De Vloo P, Fomenko A, Lee DJ, Hamani C, Munhoz RP, et al. Considerations for Patient and Target Selection in Deep Brain Stimulation Surgery for Parkinson's Disease. In: Stoker TB, Greenland JC, editors. Parkinson's Disease: Pathogenesis and Clinical Aspects, Brisbane (AU): Codon Publications; 2018.
[18] Goftari M, Kim J, Johnson E, Patriat R, Palnitkar T, Harel N, et al. Pallidothalamic tract activation predicts suppression of stimulation-induced dyskinesias in a case study of Parkinson's disease. Brain Stimulation: Basic, Translational, and Clinical Research in Neuromodulation 2020;13:1821–3. https://doi.org/10.1016/j.brs.2020.09.022.
[19] Maciel R, Soh D, Munhoz RP, Poon Y-Y, Kalia SK, Hodaie M, et al. Programming Directional Deep Brain Stimulation in Parkinson's Disease: A Randomized Prospective Trial Comparing Early versus Delayed Stimulation Steering. SFN 2021;99:484–90. https://doi.org/10.1159/000517054.
[20] Slopsema JP, Canna A, Uchenik M, Lehto LJ, Krieg J, Wilmerding L, et al. Orientation-selective and directional deep brain stimulation in swine assessed by functional MRI at 3T. NeuroImage 2021;224:117357. https://doi.org/10.1016/j.neuroimage.2020.117357.
[21] Contarino MF, Bour LJ, Verhagen R, Lourens MA, de Bie RM, van den Munckhof P, et al. Directional steering: A novel approach to deep brain stimulation. Neurology 2014;83:1163–9. https://doi.org/10.1212/WNL.0000000000000823.
[22] Chandran AS, Bynevelt M, Lind CRP. Magnetic resonance imaging of the subthalamic nucleus for deep brain stimulation. Journal of Neurosurgery 2016;124:96–105. https://doi.org/10.3171/2015.1.JNS142066.
[23] Bot M, Verhagen O, Caan M, Potters WV, Dilai Y, Odekerken VJJ, et al. Defining the Dorsal STN Border Using 7.0-T MRI: A Comparison to Microelectrode Recordings and Lower Field Strength MRI. SFN 2019;97:153–9. https://doi.org/10.1159/000500109.
[24] Milchenko M, Norris SA, Poston K, Campbell MC, Ushe M, Perlmutter JS, et al. 7T MRI subthalamic nucleus atlas for use with 3T MRI. J Med Imaging (Bellingham) 2018;5:015002. https://doi.org/10.1117/1.JMI.5.1.015002.
[25] Saleh C, Dooms G, Berthold C, Hertel F. Post-operative imaging in deep brain stimulation: A controversial issue. Neuroradiol J 2016;29:244–9. https://doi.org/10.1177/1971400916639960.
[26] Giller C, Mehta S, Yanasak N, Jenkins P. Avoidance of electrode related MRI artifact during staged deep brain stimulator implantation. J Neurol Surg A Cent Eur Neurosurg 2012;73:320–3. https://doi.org/10.1055/s-0032-1322590.
[27] JASPER HH, ANDREWS HL. ELECTRO-ENCEPHALOGRAPHY: III. NORMAL DIFFERENTIATION OF OCCIPITAL AND PRECENTRAL REGIONS IN MAN. Archives of Neurology & Psychiatry 1938;39:96–115. https://doi.org/10.1001/archneurpsyc.1938.02270010106010.
[28] Little S, Brown P. The functional role of beta oscillations in Parkinson's disease. Parkinsonism & Related Disorders 2014;20:S44–8. https://doi.org/10.1016/S1353-8020(13)70013-0.

[29] Müller EJ, Robinson PA. Suppression of Parkinsonian Beta Oscillations by Deep Brain Stimulation: Determination of Effective Protocols. Front Comput Neurosci 2018;12:98. https://doi.org/10.3389/fncom.2018.00098.
[30] Little S, Pogosyan A, Neal S, Zavala B, Zrinzo L, Hariz M, et al. Adaptive deep brain stimulation in advanced Parkinson disease: Adaptive DBS in PD. Annals of Neurology 2013;74:449–57. https://doi.org/10.1002/ana.23951.
[31] Johnson LA, Nebeck SD, Muralidharan A, Johnson MD, Baker KB, Vitek JL. Closed-Loop Deep Brain Stimulation Effects on Parkinsonian Motor Symptoms in a Non-Human Primate – Is Beta Enough? Brain Stimulation 2016;9:892–6. https://doi.org/10.1016/j.brs.2016.06.051.
[32] Kuhn AA, Doyle L, Pogosyan A, Yarrow K, Kupsch A, Schneider G-H, et al. Modulation of beta oscillations in the subthalamic area during motor imagery in Parkinson's disease 2006;129:695–706. https://doi.org/10.1093/brain/awh715.
[33] Hell F, Plate A, Mehrkens JH, Bötzel K. Subthalamic oscillatory activity and connectivity during gait in Parkinson's disease. Neuroimage Clin 2018;19:396–405. https://doi.org/10.1016/j.nicl.2018.05.001.
[34] Pani P, Di Bello F, Brunamonti E, D'Andrea V, Papazachariadis O, Ferraina S. Alpha- and beta-band oscillations subserve different processes in reactive control of limb movements. Front Behav Neurosci 2014;8:383. https://doi.org/10.3389/fnbeh.2014.00383.
[35] Zhang S, Connolly AT, Madden LR, Vitek JL, Johnson MD. High-resolution local field potentials measured with deep brain stimulation arrays. J Neural Eng 2018;15:046019. https://doi.org/10.1088/1741-2552/aabdf5.
[36] Horn A, Neumann W, Degen K, Schneider G, Kühn AA. Toward an electrophysiological "sweet spot" for deep brain stimulation in the subthalamic nucleus. Hum Brain Mapp 2017;38:3377–90. https://doi.org/10.1002/hbm.23594.
[37] Koirala N, Serrano L, Paschen S, Falk D, Anwar AR, Kuravi P, et al. Mapping of subthalamic nucleus using microelectrode recordings during deep brain stimulation. Sci Rep 2020;10:19241. https://doi.org/10.1038/s41598-020-74196-5.
[38] Snellings A, Sagher O, Anderson DJ, Aldridge JW. Identification of the subthalamic nucleus in deep brain stimulation surgery with a novel wavelet-derived measure of neural background activity. J Neurosurg 2009;111:767–74. https://doi.org/10.3171/2008.11.JNS08392.
[39] Lu CW, Malaga KA, Chou KL, Chestek CA, Patil PG. High density microelectrode recording predicts span of therapeutic tissue activation volumes in subthalamic deep brain stimulation for Parkinson disease. Brain Stimulation 2020;13:412–9. https://doi.org/10.1016/j.brs.2019.11.013.
[40] Parker JL, Shariati NH, Karantonis DM. Electrically evoked compound action potential recording in peripheral nerves. Bioelectronics in Medicine 2018;1:71–83. https://doi.org/10.2217/bem-2017-0005.
[41] Parker JL, Obradovic M, Hesam Shariati N, Gorman RB, Karantonis DM, Single PS, et al. Evoked Compound Action Potentials Reveal Spinal Cord Dorsal Column Neuroanatomy. Neuromodulation: Technology at the Neural Interface 2020;23:82–95. https://doi.org/10.1111/ner.12968.
[42] Russo M, Brooker C, Cousins MJ, Taylor N, Boesel T, Sullivan R, et al. Sustained Long-Term Outcomes With Closed-Loop Spinal Cord Stimulation: 12-Month

Results of the Prospective, Multicenter, Open-Label Avalon Study. Neurosurgery 2020;87:E485–95. https://doi.org/10.1093/neuros/nyaa003.
[43] Parker JL, Karantonis DM, Single PS, Obradovic M, Laird J, Gorman RB, et al. Electrically Evoked Compound Action Potentials Recorded From the Sheep Spinal Cord. Neuromodulation: Technology at the Neural Interface 2013;16:295–303. https://doi.org/10.1111/ner.12053.
[44] Jeon EK, Brown CJ, Etler CP, O'Brien S, Chiou L-K, Abbas PJ. Comparison of Electrically Evoked Compound Action Potential Thresholds and Loudness Estimates for the Stimuli Used to Program the Advanced Bionics Cochlear Implant. J Am Acad Audiol 2010;21:016–27. https://doi.org/10.3766/jaaa.21.1.3.
[45] Miller CA, Brown CJ, Abbas PJ, Chi S-L. The clinical application of potentials evoked from the peripheral auditory system. Hearing Research 2008;242:184–97. https://doi.org/10.1016/j.heares.2008.04.005.
[46] Adenis V, Gourévitch B, Mamelle E, Recugnat M, Stahl P, Gnansia D, et al. ECAP growth function to increasing pulse amplitude or pulse duration demonstrates large inter-animal variability that is reflected in auditory cortex of the guinea pig. PLOS ONE 2018;13:e0201771. https://doi.org/10.1371/journal.pone.0201771.
[47] Gärtner L, Lenarz T, Büchner A. Fine-grain recordings of the electrically evoked compound action potential amplitude growth function in cochlear implant recipients. Biomed Eng Online 2018;17:140. https://doi.org/10.1186/s12938-018-0588-z.
[48] Finn WE, LoPresti PG. Wavelength and intensity dependence of retinal evoked responses using in vivo optic nerve recording. IEEE Transactions on Neural Systems and Rehabilitation Engineering 2003;11:372–6. https://doi.org/10.1109/TNSRE.2003.819928.
[49] Maynard et al. Nitric oxide modulates light-evoked compound action potentials in the intact rabbit retina. Lippincott-Raven Publishers 1995;6:850–2.
[50] Schmidt SL, Brocker DT, Swan BD, Turner DA, Grill WM. Evoked potentials reveal neural circuits engaged by human deep brain stimulation. Brain Stimulation 2020;13:1706–18. https://doi.org/10.1016/j.brs.2020.09.028.
[51] Gmel GE, Hamilton TJ, Obradovic M, Gorman RB, Single PS, Chenery HJ, et al. A new biomarker for subthalamic deep brain stimulation for patients with advanced Parkinson's disease--a pilot study. J Neural Eng 2015;12:066013. https://doi.org/10.1088/1741-2560/12/6/066013.
[52] Kent AR, Grill WM. Neural origin of evoked potentials during thalamic deep brain stimulation. J Neurophysiol 2013;110:826–43. https://doi.org/10.1152/jn.00074.2013.
[53] Buzsáki G, Anastassiou CA, Koch C. The origin of extracellular fields and currents — EEG, ECoG, LFP and spikes. Nat Rev Neurosci 2012;13:407–20. https://doi.org/10.1038/nrn3241.
[54] Kent AR, Grill WM. Recording evoked potentials during deep brain stimulation: development and validation of instrumentation to suppress the stimulus artefact. J Neural Eng 2012;9:036004. https://doi.org/10.1088/1741-2560/9/3/036004.
[55] Cohen LT, Richardson LM, Saunders E, Cowan RSC. Spatial spread of neural excitation in cochlear implant recipients: comparison of improved ECAP method

and psychophysical forward masking. Hearing Research 2003;179:72–87. https://doi.org/10.1016/S0378-5955(03)00096-0.
[56] Tang Q, Benítez R, Zeng F-G. Spatial channel interactions in cochlear implants. J Neural Eng 2011;8:046029. https://doi.org/10.1088/1741-2560/8/4/046029.
[57] Somers B, Long CJ, Francart T. EEG-based diagnostics of the auditory system using cochlear implant electrodes as sensors. Sci Rep 2021;11:5383. https://doi.org/10.1038/s41598-021-84829-y.
[58] Sanabria DE, Johnson LA, Yu Y, Busby Z, Nebeck S, Zhang J, et al. Real-time suppression and amplification of frequency-specific neural activity using stimulation evoked oscillations. Brain Stimulation: Basic, Translational, and Clinical Research in Neuromodulation 2020;13:1732–42. https://doi.org/10.1016/j.brs.2020.09.017.
[59] Brinda AK, Doyle AM, Blumenfeld M, Krieg J, Alisch JSR, Spencer C, et al. Longitudinal analysis of local field potentials recorded from directional deep brain stimulation lead implants in the subthalamic nucleus. J Neural Eng 2021;18:046050. https://doi.org/10.1088/1741-2552/abfc1c.
[60] Vitek JL, Johnson LA. Understanding Parkinson's disease and deep brain stimulation: Role of monkey models. Proceedings of the National Academy of Sciences 2019;116:26259–65. https://doi.org/10.1073/pnas.1902300116.
[61] Miocinovic S, Parent M, Butson CR, Hahn PJ, Russo GS, Vitek JL, et al. Computational analysis of subthalamic nucleus and lenticular fasciculus activation during therapeutic deep brain stimulation. J Neurophysiol 2006;96:1569–80. https://doi.org/10.1152/jn.00305.2006.
[62] Imbert C, Bezard E, Guitraud S, Boraud T, Gross CE. Comparison of eight clinical rating scales used for the assessment of MPTP-induced parkinsonism in the Macaque monkey. Journal of Neuroscience Methods 2000;96:71–6.
[63] Meissner W, Leblois A, Hansel D, Bioulac B, Gross CE, Benazzouz A, et al. Subthalamic high frequency stimulation resets subthalamic firing and reduces abnormal oscillations. Brain 2005;128:2372–82. https://doi.org/10.1093/brain/awh616.
[64] Kent AR, Swan BD, Brocker DT, Turner DA, Gross RE, Grill WM. Measurement of evoked potentials during thalamic deep brain stimulation. Brain Stimul 2015;8:42–56. https://doi.org/10.1016/j.brs.2014.09.017.
[65] Butson CR, Cooper SE, Henderson JM, McIntyre CC. Patient-Specific Analysis of the Volume of Tissue Activated During Deep Brain Stimulation. Neuroimage 2007;34:661–70. https://doi.org/10.1016/j.neuroimage.2006.09.034.
[66] Goftari M, Lu C, Schmidt M, Patriat R, Palnitkar T, Kim J, et al. Parkinsonian gait effects with DBS are associated with pallido-peduncular axis activation. BioRxiv 2021:2021.10.13.464270. https://doi.org/10.1101/2021.10.13.464270.
[67] Strelow JN, Baldermann JC, Dembek TA, Jergas H, Petry-Schmelzer JN, Schott F, et al. Structural connectivity of subthalamic nucleus stimulation for improving freezing of gait. MedRxiv 2021:2021.07.01.21259612. https://doi.org/10.1101/2021.07.01.21259612.
[68] He C, Zhang F, Li L, Jiang C, Li L. Measurement of Lead Localization Accuracy Based on Magnetic Resonance Imaging. Frontiers in Neuroscience 2021;15.

[69] Darcy N, Lofredi R, Al-Fatly B, Neumann W-J, Hübl J, Brücke C, et al. Spectral and spatial distribution of subthalamic beta peak activity in Parkinson's disease patients. Experimental Neurology 2022:114150. https://doi.org/10.1016/j.expneurol.2022.114150.
[70] He S, Teagle HFB, Buchman CA. The Electrically Evoked Compound Action Potential: From Laboratory to Clinic. Frontiers in Neuroscience 2017;11.
[71] Johnson MD, Miocinovic S, McIntyre CC, Vitek JL. Mechanisms and targets of deep brain stimulation in movement disorders. Neurotherapeutics 2008;5:294–308. https://doi.org/10.1016/j.nurt.2008.01.010.
[72] Hashimoto T, Elder CM, Okun MS, Patrick SK, Vitek JL. Stimulation of the Subthalamic Nucleus Changes the Firing Pattern of Pallidal Neurons. J Neurosci 2003;23:1916–23.
[73] Agnesi F, Muralidharan A, Baker KB, Vitek JL, Johnson MD. Fidelity of frequency and phase entrainment of circuit-level spike activity during DBS. Journal of Neurophysiology 2015;114:825–34. https://doi.org/10.1152/jn.00259.2015.
[74] Filali M, Hutchison WD, Palter VN, Lozano AM, Dostrovsky JO. Stimulation-induced inhibition of neuronal firing in human subthalamic nucleus. Exp Brain Res 2004;156:274–81. https://doi.org/10.1007/s00221-003-1784-y.
[75] Zaidel A, Spivak A, Grieb B, Bergman H, Israel Z. Subthalamic span of beta oscillations predicts deep brain stimulation efficacy for patients with Parkinson's disease. Brain 2010;133:2007–21. https://doi.org/10.1093/brain/awq144.
[76] Hartmann CJ, Fliegen S, Groiss SJ, Wojtecki L, Schnitzler A. An update on best practice of deep brain stimulation in Parkinson's disease. Ther Adv Neurol Disord 2019;12:1756286419838096. https://doi.org/10.1177/1756286419838096.
[77] Rosa M, Giannicola G, Servello D, Marceglia S, Pacchetti C, Porta M, et al. Subthalamic Local Field Beta Oscillations during Ongoing Deep Brain Stimulation in Parkinson's Disease in Hyperacute and Chronic Phases. Neurosignals 2011;19:151–62. https://doi.org/10.1159/000328508.
[78] Escobar Sanabria D, Aman JE, Zapata Amaya V, Johnson LA, Farooqi H, Wang J, et al. Controlling pallidal oscillations in real-time in Parkinson's disease using evoked interference deep brain stimulation (eiDBS): Proof of concept in the human. Brain Stimulation 2022;15:1111–9. https://doi.org/10.1016/j.brs.2022.07.047.
[79] Blahak C, Bäzner H, Capelle H-H, Wöhrle JC, Weigel R, Hennerici MG, et al. Rapid response of parkinsonian tremor to STN-DBS changes: direct modulation of oscillatory basal ganglia activity? Mov Disord 2009;24:1221–5. https://doi.org/10.1002/mds.22536.
[80] Temperli P, Ghika J, Villemure JG, Burkhard PR, Bogousslavsky J, Vingerhoets FJ. How do parkinsonian signs return after discontinuation of subthalamic DBS? Neurology 2003;60:78–81.
[81] Lopiano L, Torre E, Benedetti F, Bergamasco B, Perozzo P, Pollo A, et al. Temporal Changes in Movement Time during the Switch of the Stimulators in Parkinson's Disease Patients Treated by Subthalamic Nucleus Stimulation. European Neurology 2003;50:94–9. https://doi.org/10.1159/000072506.
[82] Moran A, Stein E, Tischler H, Belelovsky K, Bar-Gad I. Dynamic Stereotypic Responses of Basal Ganglia Neurons to Subthalamic Nucleus High-Frequency Stimulation in the Parkinsonian Primate. Frontiers in Systems Neuroscience 2011;5.

[83] Durand DM, Park E-H, Jensen AL. Potassium diffusive coupling in neural networks. Philos Trans R Soc Lond B Biol Sci 2010;365:2347–62. https://doi.org/10.1098/rstb.2010.0050.
[84] Michelson NJ, Eles JR, Vazquez AL, Ludwig KA, Kozai TD. Calcium activation of cortical neurons by continuous electrical stimulation: Frequency-dependence, temporal fidelity and activation density. J Neurosci Res 2019;97:620–38. https://doi.org/10.1002/jnr.24370.
[85] Geiger JRP, Jonas P. Dynamic Control of Presynaptic Ca2+ Inflow by Fast-Inactivating K+ Channels in Hippocampal Mossy Fiber Boutons. Neuron 2000;28:927–39. https://doi.org/10.1016/S0896-6273(00)00164-1.
[86] Brody DL, Yue DT. Release-Independent Short-Term Synaptic Depression in Cultured Hippocampal Neurons. J Neurosci 2000;20:2480–94. https://doi.org/10.1523/JNEUROSCI.20-07-02480.2000.
[87] Sato F, Parent M, Levesque M, Parent A. Axonal branching pattern of neurons of the subthalamic nucleus in primates. J Comp Neurol 2000;424:142–52. https://doi.org/10.1002/1096-9861(20000814)424:1<142::aid-cne10>3.0.co;2-8.
[88] Kocsis JD, Malenka RC, Waxman SG. Effects of extracellular potassium concentration on the excitability of the parallel fibres of the rat cerebellum. J Physiol 1983;334:225–44.
[89] Galarreta M, Hestrin S. Frequency-dependent synaptic depression and the balance of excitation and inhibition in the neocortex. Nat Neurosci 1998;1:587–94. https://doi.org/10.1038/2822.
[90] Chance FS, Nelson SB, Abbott LF. Synaptic Depression and the Temporal Response Characteristics of V1 Cells. J Neurosci 1998;18:4785–99. https://doi.org/10.1523/JNEUROSCI.18-12-04785.1998.
[91] Ohzawa I, Sclar G, Freeman RD. Contrast gain control in the cat's visual system. Journal of Neurophysiology 1985;54:651–67. https://doi.org/10.1152/jn.1985.54.3.651.
[92] Boudkkazi S, Fronzaroli-Molinieres L, Debanne D. Presynaptic action potential waveform determines cortical synaptic latency. The Journal of Physiology 2011;589:1117. https://doi.org/10.1113/jphysiol.2010.199653.
[93] Chung YH, Shin C, Kim MJ, Cha CI. Immunohistochemical study on the distribution of six members of the Kv1 channel subunits in the rat basal ganglia. Brain Research 2000;875:164–70. https://doi.org/10.1016/S0006-8993(00)02586-5.
[94] Perera T, Lee W-L, Jones M, Tan JL, Proud EL, Begg A, et al. A palm-worn device to quantify rigidity in Parkinson's disease. Journal of Neuroscience Methods 2019;317:113–20. https://doi.org/10.1016/j.jneumeth.2019.02.006.
[95] Cooper SE, Driesslein KG, Noecker AM, McIntyre CC, Machado AM, Butson CR. Anatomical Targets Associated with Abrupt versus Gradual Washout of Subthalamic Deep Brain Stimulation Effects on Bradykinesia. PLoS ONE 2014;9:e99663. https://doi.org/10.1371/journal.pone.0099663.
[96] Harmsen IE, Fernandes FW, Krauss JK, Lozano AM. Where Are We with Deep Brain Stimulation? A Review of Scientific Publications and Ongoing Research. SFN 2022;100:184–97. https://doi.org/10.1159/000521372.
[97] Martens HC, Toader E, Decre MM, Anderson DJ, Vetter R, Kipke DR, et al. Spatial steering of deep brain stimulation volumes using a novel lead design. Clinical

Neurophysiology : Official Journal of the International Federation of Clinical Neurophysiology 2011;122:558–66. https://doi.org/10.1016/j.clinph.2010.07.026.
[98] Pollo C, Kaelin-Lang A, Oertel MF, Stieglitz L, Taub E, Fuhr P, et al. Directional deep brain stimulation: an intraoperative double-blind pilot study. Brain : A Journal of Neurology 2014;137:2015–26. https://doi.org/10.1093/brain/awu102.
[99] Connolly AT, Vetter RJ, Hetke JF, Teplitzky BA, Kipke DR, Pellinen DS, et al. A Novel Lead Design for Modulation and Sensing of Deep Brain Structures. IEEE Transactions on Biomedical Engineering 2016;63:148–57. https://doi.org/10.1109/TBME.2015.2492921.
[100] Dembek TA, Reker P, Visser-Vandewalle V, Wirths J, Treuer H, Klehr M, et al. Directional DBS increases side-effect thresholds-A prospective, double-blind trial: Directional Dbs Increases Side-Effect Thresholds. Movement Disorders 2017;32:1380–8. https://doi.org/10.1002/mds.27093.
[101] Toader E, Decre MM, Martens HC. Steering deep brain stimulation fields using a high resolution electrode array. Conference Proceedings : . Annual International Conference of the IEEE Engineering in Medicine and Biology Society IEEE Engineering in Medicine and Biology Society Conference 2010;2010:2061–4. https://doi.org/10.1109/IEMBS.2010.5626472.
[102] Zhang S, Connolly AT, Madden LR, Vitek JL, Johnson MD. High-resolution local field potentials measured with deep brain stimulation arrays. J Neural Eng 2018;15:046019. https://doi.org/10.1088/1741-2552/aabdf5.
[103] Woods V, Trumpis M, Bent B, Palopoli-Trojani K, Chiang C-H, Wang C, et al. Long-term recording reliability of liquid crystal polymer μECoG arrays. J Neural Eng 2018;15:066024. https://doi.org/10.1088/1741-2552/aae39d.
[104] Frisk L, Parviainen A, Kokko K. Liquid crystal polymer as a substrate material for flip chip ACA interconnections. 3rd Electronics System Integration Technology Conference ESTC, 2010, p. 1–6. https://doi.org/10.1109/ESTC.2010.5642913.
[105] Ordonez JS, Rudmann L, Cvancara P, Bentler C, Stieglitz T. Mechanical deformation of thin film platinum under electrical stimulation. 2015 37th Annual International Conference of the IEEE Engineering in Medicine and Biology Society (EMBC), 2015, p. 1045–8. https://doi.org/10.1109/EMBC.2015.7318544.
[106] Motta PS, Judy JW. Multielectrode microprobes for deep-brain stimulation fabricated with a customizable 3-D electroplating process. IEEE Transactions on Biomedical Engineering 2005;52:923–33. https://doi.org/10.1109/TBME.2005.845225.
[107] Green RA, Matteucci PB, Dodds CWD, Palmer J, Dueck WF, Hassarati RT, et al. Laser patterning of platinum electrodes for safe neurostimulation. J Neural Eng 2014;11:056017. https://doi.org/10.1088/1741-2560/11/5/056017.
[108] Hyakumura T, Aregueta-Robles U, Duan W, Villalobos J, Adams WK, Poole-Warren L, et al. Improving Deep Brain Stimulation Electrode Performance in vivo Through Use of Conductive Hydrogel Coatings. Front Neurosci 2021;15:761525. https://doi.org/10.3389/fnins.2021.761525.
[109] Petrossians A, Whalen JJ, Weiland JD, Mansfeld F. Surface modification of neural stimulating/recording electrodes with high surface area platinum-iridium alloy coatings. 2011 Annual International Conference of the IEEE Engineering in

Medicine and Biology Society, 2011, p. 3001–4. https://doi.org/10.1109/IEMBS.2011.6090823.
[110] Petrossians A, Whalen JJ, Weiland JD, Mansfeld F. Electrodeposition and Characterization of Thin-Film Platinum-Iridium Alloys for Biological Interfaces. J Electrochem Soc 2011;158:D269. https://doi.org/10.1149/1.3559477.
[111] Zfit n.d. https://www.mathworks.com/matlabcentral/fileexchange/19460-zfit (accessed September 21, 2022).
[112] Jeong J, Bae SH, Seo J-M, Chung H, Kim SJ. Long-term evaluation of a liquid crystal polymer (LCP)-based retinal prosthesis. J Neural Eng 2016;13:025004. https://doi.org/10.1088/1741-2560/13/2/025004.
[113] LaRoy JJL, Teplitzky BA, Johnson MD. Multitine deep brain stimulation leads to shape neural activation in three dimensions. Journal of Medical Devices, Transactions of the ASME 2014;8. https://doi.org/10.1115/1.4027022.
[114] Cogan SF, Ludwig KA, Welle CG, Takmakov P. Tissue damage thresholds during therapeutic electrical stimulation. Journal of Neural Engineering 2016;13:021001. https://doi.org/10.1088/1741-2560/13/2/021001.
[115] Miller KJ, Müller K-R, Valencia GO, Huang H, Gregg NM, Worrell GA, et al. Canonical Response Parameterization: Quantifying the structure of responses to single-pulse intracranial electrical brain stimulation 2022:2022.08.05.502944. https://doi.org/10.1101/2022.08.05.502944.
[116] Thevathasan W, Sinclair NC, Bulluss KJ, McDermott HJ. Tailoring Subthalamic Nucleus Deep Brain Stimulation for Parkinson's Disease Using Evoked Resonant Neural Activity. Frontiers in Human Neuroscience 2020;14.
[117] Sinclair NC, McDermott HJ, Bulluss KJ, Fallon JB, Perera T, Xu SS, et al. Subthalamic Nucleus Deep Brain Stimulation Evokes Resonant Neural Activity. Ann Neurol 2018;83:1027–31. https://doi.org/10.1002/ana.25234.
[118] Foutz TJ, McIntyre CC. Evaluation of novel stimulus waveforms for deep brain stimulation. Journal of Neural Engineering 2010;7:066008. https://doi.org/10.1088/1741-2560/7/6/066008.
[119] Akbar U, Raike RS, Hack N, Hess CW, Skinner J, Martinez-Ramirez D, et al. Randomized, Blinded Pilot Testing of Nonconventional Stimulation Patterns and Shapes in Parkinson's Disease and Essential Tremor: Evidence for Further Evaluating Narrow and Biphasic Pulses. Neuromodulation 2016;19:343–56. https://doi.org/10.1111/ner.12397.
[120] Almeida L, Martinez-Ramirez D, Ahmed B, Deeb W, Jesus SD, Skinner J, et al. A pilot trial of square biphasic pulse deep brain stimulation for dystonia: The BIP dystonia study. Mov Disord 2017;32:615–8. https://doi.org/10.1002/mds.26906.